ESA STUDY CONTRACT REPORT –

Deliverable D 2.2

Numerical and analytical sandwich structure analysis-technical note

ESA Contract No: **400114452/15/ NL/NDe**	SUBJECT: **Milestone 4, D 2.2** **Numerical and analytical sandwich structure analysis**	CONTRACTOR: **Riga Technical University, Institute of Materials and Structures**
* ESA CR( )No:	No. of Volumes:1 This is Volume No:1	CONTRACTOR'S REFERENCE: **62518 (bidder code)**

ABSTRACT:

A current report summarise efforts in development of numerical analysis procedures which has been verified analyticaly and validated with initial experimental tests. All numerical analysis are implemented in commercial finite element software code ANSYS by scripting APDL log files. Where main emphasis was focused on barely visible damage (BVID) introduction by indentation and estimation of residual dent depth and accumulated strains. While numerical methods capture all variety of boundary conditions, layup and honeycomb orientation as well as geometrical and material nonlienarities the analytical approach assumes symmetry and equiivalent load distribution around dent. Both initial verification and final validation was performed in line with selected physical experiments. This include a reverse identification of reference panel performance assessment by self frequency tests and modal analyses. At the current stage we have achieved very good correlation among dozen of currently tested indented specimens by assessing residual dent (barely visible damage) those achievements are uploaded on project web page under section of preliminary design tools (bnm4eks.rtu.lv). A further validation of panel residual strength will be in incorporated in elaboration of design tool and update of numerical desing guideline deliveriable.

The work described in this report was done under ESA Contract. Responsibility for the contents resides in the author or organisation that prepared it.
Names of authors: Kaspars Kalniņš; Guntis Japiņš; Eduards Skuķis; Oļģerts Ozoliņš, Jānis Andersons, Gints Jēkabsons.

** NAME OF ESA STUDY MANAGER: DIV: DIRECTORATE:	** ESA BUDGET HEADING:

RIGA TECHNICAL UNIVERSITY
IMS
INSTITUTE OF MATERIALS AND STRUCTURES

Institute of Materials and Structures
Rīga, Ķīpsalas iela 6A, LV-1048
Tel. +371 67089124
Web. http://www.ims.rtu.lv

Table of contents

RIGA TECHNICAL UNIVERSITY

IMS

INSTITUTE OF MATERIALS AND STRUCTURES

Institute of Materials and Structures
Rīga, Ķīpsalas iela 6A, LV-1048
Tel. +371 67089124
Web. http://www.ims.rtu.lv

Table of figures

RIGA TECHNICAL UNIVERSITY

INSTITUTE OF MATERIALS AND STRUCTURES

Institute of Materials and Structures
Rīga, Ķīpsalas iela 6A, LV-1048
Tel. +371 67089124
Web. http://www.ims.rtu.lv

Introduction

A current report summarise efforts and lessons learned in order to develop and validate the numerical simulation model by commercial finite element code ANSYS [1]. The modelling include a finite element type, mesh as well as selected material property sensitivity analysis. For element type studies both shell only and shell/solid elements types has been investigated. In order to find best trade-off between model prediction reliability and CPU timing a mesh sensitivity have been studied for both element type models. A shell bounded by solid model have been identified as most appropriate as both CPU time and robustness of the solution are in trade off with physical experiment. It should be noted that actual honeycomb model has been replaced with equivalent – volume representative elements which accounts for models nonlinearities which is partly linked with plasticity of aluminium foil. The validation.

Initially while only few specimens where build the verification phase included numerical modal analysis only. This early verification step allowed to update analysis strategy in early stage of development. From numerical simulation point of view linear analyses are very robust and fast therefore simple in verification of assumptions included in numerical analysis.

It has been followed by more sophisticated finite element model consisted of shell/solid modelled honeycomb structure, covered by two CFRP shell face sheets. Model incorporates tied face sheet to honeycomb connection by sheared nodes, thus eliminating possible skin delamination damage propagation. Due to presence of buckling of honeycomb cell walls minimum element size was determined to be set as ½ of the cell size (1.5 mm), to allow the walls to form buckles. Adhesive layer added to the skin lay-up as additional layer with corresponding material properties and material plasticity model. Honeycomb structure model has been set to incorporate multilinear isotropic hardening plasticity material model based on experimental characterization. Moreover composite progressive damage model was integrated, based on characterization of material properties of UD composite. Composite progressive damage model realized through max stress criteria with material stiffness degradation. Interaction between indenter and panel surface was modelled as surface-to-surface contact.

Finally both numerical and analytical approach for identation of sandwich panel have been validated with physical experiments and full range of results have been uploaded on projects web page: http://bnm4eks.rtu.lv/tools_en.html. Several further steps have been identified and will be incorporated in final deliveriable focusing on numerical analysis best design practice.

RIGA TECHNICAL UNIVERSITY
IMS
INSTITUTE OF MATERIALS AND STRUCTURES

Institute of Materials and Structures
Rīga, Ķīpsalas iela 6A, LV-1048
Tel. +371 67089124
Web. http://www.ims.rtu.lv

1   General consideration in development of numerical model

1.1   Numerical model development based on finite element method

Current report focusing on development of sandwich honeycomb structure to be modelled by commercial finite element method (FEM) code. Assumptions to be integrated in numerical model are graphically shown in Figure 1.1. Originally model consist of two relatively thin skins, aluminium honeycomb sandwich core and adhesive layers bounding them together. In numerical model all, geometrical, material and element assumptions should be considered as parametrical input variables. This allowing user to modify ply stacking sequence and thickness of all layers, as well as panel length, width and height in line with honeycomb topology. Material properties including orthotropic stiffness constants and plasticity for aluminium thin wall core or adhesive bounding layer viscoelasticity should be considered in numerical analysis.
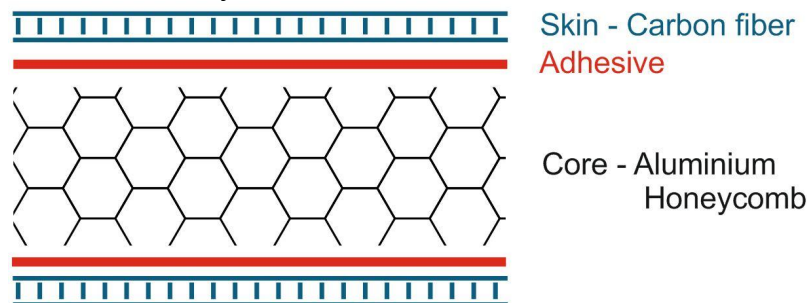
Figure 1.1. Schematic structure of sandwich panel.

While numerically modelling structure a particular attention should be devoted to trade-off between FEM mesh size and CPU time. A uniform mesh fine is expected to be most accurate, nevertheless considering local defects on full scale panels are extremely time-costly thus balance should be found. An example of expected FEM numerical model are shown in Figure 1.2. Initial model should be double checked for numerous sources of errors including local orientation of elements (Figure 1.2 a/b) which assures correct assumptions of stacking sequence and material properties.

a)   b)
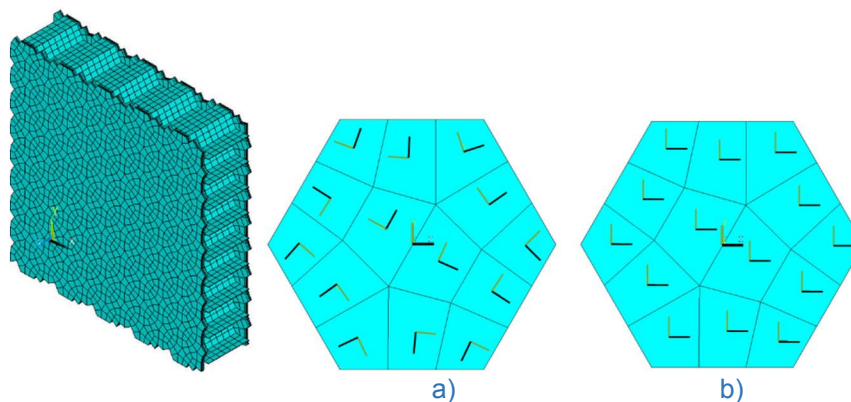
Figure 1.2. Expected fine mesh detailed finite element model of sandwich panel; a) disorderly orientated elements; b) aligned orientation of elements.

5

RIGA TECHNICAL UNIVERSITY
IMS
INSTITUTE OF MATERIALS AND STRUCTURES

Institute of Materials and Structures
Rīga, Ķīpsalas iela 6A, LV-1048
Tel. +371 67089124
Web. http://www.ims.rtu.lv

Initial finite element mesh size correlation have to be revisited during verification steps and validation stage. Such practice would guarantee efficiency and robustness of developed model. Figure 1.3. outlines core layer height mesh size correlation where drastic drop of self frequency are associated with refinement of FE mesh to level of 3 and 2 mm. Therefore concluding that most robust and performance driven solution is to stay with element length of 3 mm. These considerations are implemented in current effort in development and validation of numerical and analytical sandwich structure analysis practice.
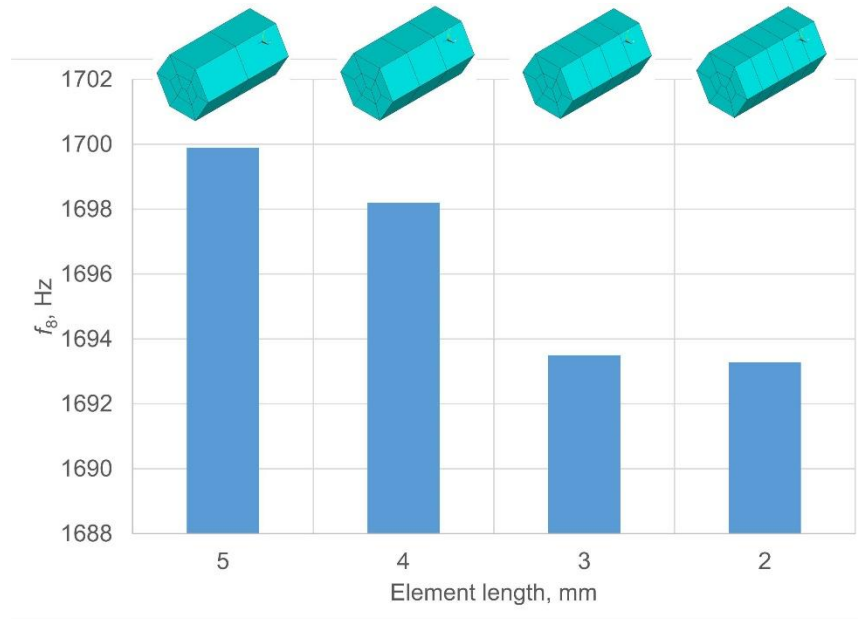
Figure 1.3. Correlation of FEM element mesh size.

1.2 Element type assumptions

Whether shell or solid element type assumption should be considered for numerical analyses. Nevertheless both alternative approaches gives a lot of variety how numerical model should be finally conducted. If sandwich structure is entirely build from shells including topology of honeycomb the model consist of extremely large number of elements (Figure 1.4). On contrary shell model allows on simple geometry to integrate several layers including honeycomb core and adhesive layer (Figure 1.5). Having such an approach restricts introduction and assessment of residual indent, while for other applications with multi ply interference (Figure 1.6) this approach is considered as most efficient. To simulate indent and to reduce complexity of model a solid introduction as layer between plies (Figure 1.7) are more ingenious approach compared to fully solid element (Figure 1.8) model. As in particularly of thin walled structures solids are not suited to represent stacking sequence of skin. Most advanced and currently widely used approach is to combine both shell element structure in are of indent and "rest" of model are made of solid element core (Figure 1.9).

6

RIGA TECHNICAL UNIVERSITY
IMS
INSTITUTE OF MATERIALS AND STRUCTURES

Institute of Materials and Structures
Rīga, Ķīpsalas iela 6A, LV-1048
Tel. +371 67089124
Web. http://www.ims.rtu.lv

1.2.1 Shell element SHELL 281

Commercial FEM code ANSYS [1]. most advanced shell element SHELL 281 is dedicated for analysing thin to moderately-thick shell structures. The element has eight nodes with six degrees of freedom at each node: translations in the x, y, and z axes, and rotations about the x, y, and z-axes. (When using the membrane option, the element has translational degrees of freedom only). SHELL 281 is well-suited for full range of applications: linear, large rotation, and/or large strain nonlinear analyses. This include a change in shell thickness to be accounted in nonlinear analyses. The element accounts of load stiffness caused redistribution of surface pressure. SHELL 281 may be used for layered applications for modelling composite shells or sandwich construction. The accuracy in modelling composite shells is governed by the first-order shear-deformation theory (usually referred to as Mindlin-Reissner shell theory).The element formulation is based on logarithmic strain and true stress measures. The element kinematics allow for finite membrane strains (stretching). However, the curvature changes within a time increment are assumed to be small.
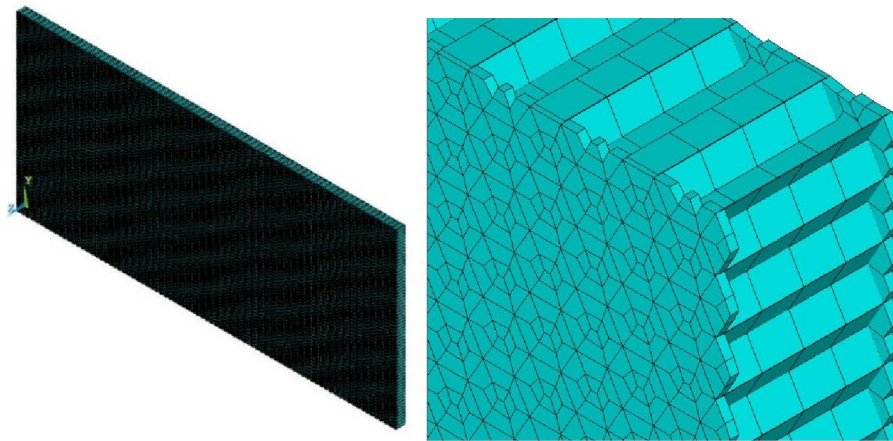
Figure 1.4. Detailed shell only model.
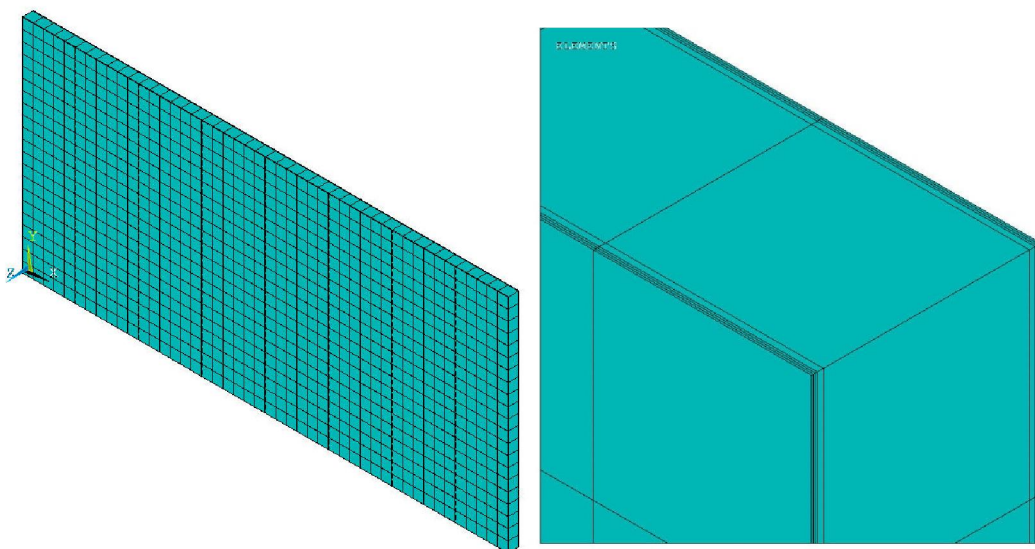
Figure 1.5. Simple shell with layup model.

RIGA TECHNICAL UNIVERSITY

IMS

INSTITUTE OF MATERIALS AND STRUCTURES

Institute of Materials and Structures
Rīga, Ķīpsalas iela 6A, LV-1048
Tel. +371 67089124
Web. http://www.ims.rtu.lv

a)   b)
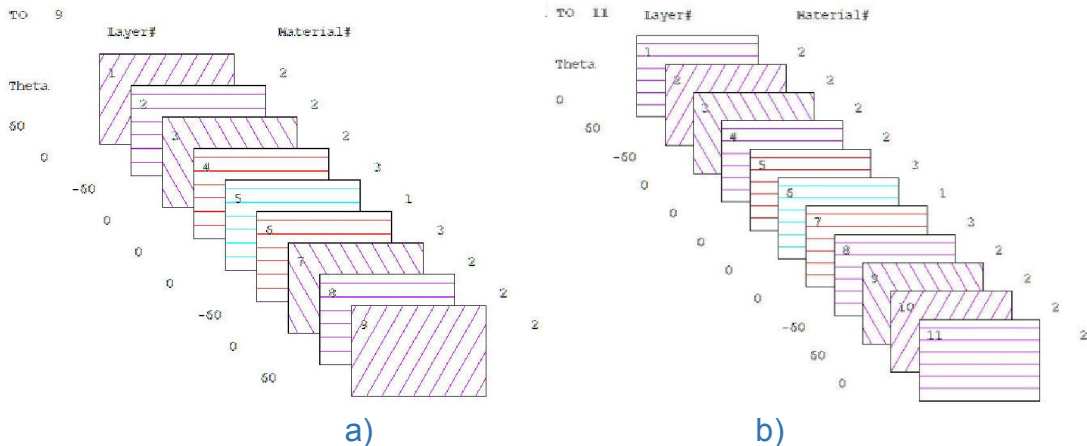
Figure 1.6. Simple shell with layup model – stacking sequence examples:
a) Lay-up of ESA_007 panel, b) Lay-up by ESA_016 panel.

1.2.2 Solid element SOLID186

SOLID186 is a higher order 3-D 20-node solid element that exhibits quadratic displacement behaviour. The element is defined by 20 nodes having three degrees of freedom per node: translations in the nodal x, y, and z directions. The element supports plasticity, hyperelasticity, creep, stress stiffening, large deflection, and large strain capabilities. It also has mixed formulation capability for simulating deformations of nearly incompressible elastoplastic materials, and fully incompressible hyperelastic materials. It should be noted that compared with simple shell with stacking sequence the degrees of freedom per model are by magnitude lower than shell only model (Figure 1.4). Nevertheless refinement of solid element in area of indent are quite complex and should be advanced with caution. Substitution of the real honeycomb by the volume formed by structural solid elements (SOLID 187), Figure 1.7, are integrated considering Hill plasticity behaviour of core elements. The fact that honeycomb structure has considerably higher stiffness and plasticity properties for transverse (through thickness) axis in comparison to in-plane properties, this has been realized through use of Hill plasticity rule. Reduced finite element model also considered as model which incorporate possible face sheet delamination model, by incorporating cohesive zone material de-bounding contact between face sheets and core volume. As well as, incorporating plasticity model for assembling adhesive layer.

RIGA TECHNICAL UNIVERSITY
IMS
INSTITUTE OF MATERIALS AND STRUCTURES

Institute of Materials and Structures
Rīga, Ķīpsalas iela 6A, LV-1048
Tel. +371 67089124
Web. http://www.ims.rtu.lv
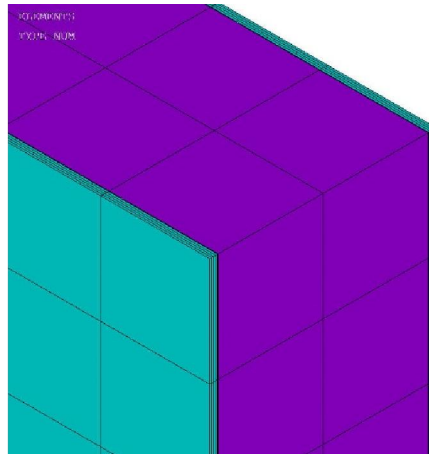
Figure 1.7. Solid and shell model
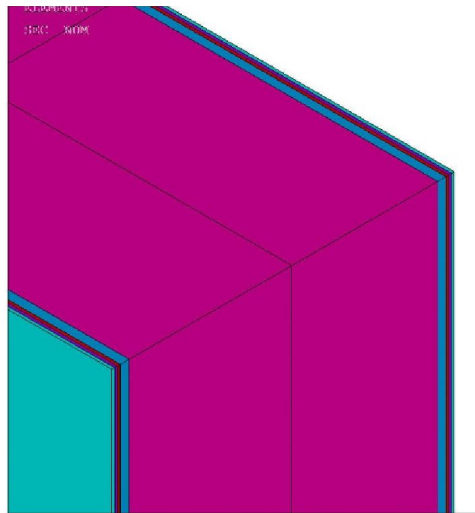
Figure 1.8. Solid only model
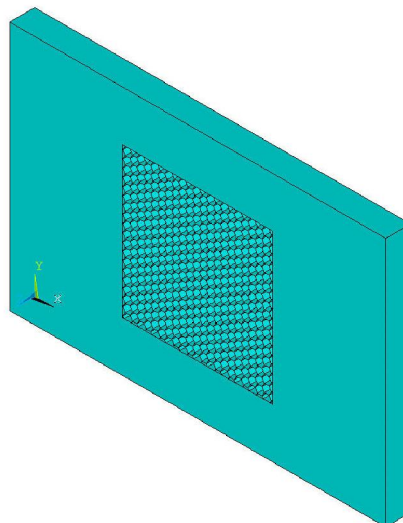
Figure 1.9. Advanced solid and shell model

RIGA TECHNICAL UNIVERSITY

IMS

INSTITUTE OF MATERIALS AND STRUCTURES

Institute of Materials and Structures
Rīga, Ķīpsalas iela 6A, LV-1048
Tel. +371 67089124
Web. http://www.ims.rtu.lv

1.2.1 Contact element

Indentation interaction between the impactor and the panel was modelled the same way as for full model by the use of surface-to-surface contact elements. The contact element size was estimated by mesh size correlation process and 1.5 mm step chosen. For all models involving contact interaction between indenter rigid body and panel surface was modelled as deformable surfaces-to-surface contact, employing surface contact elements TARGE 170 and CONTA174 in ANSYS commercial software.
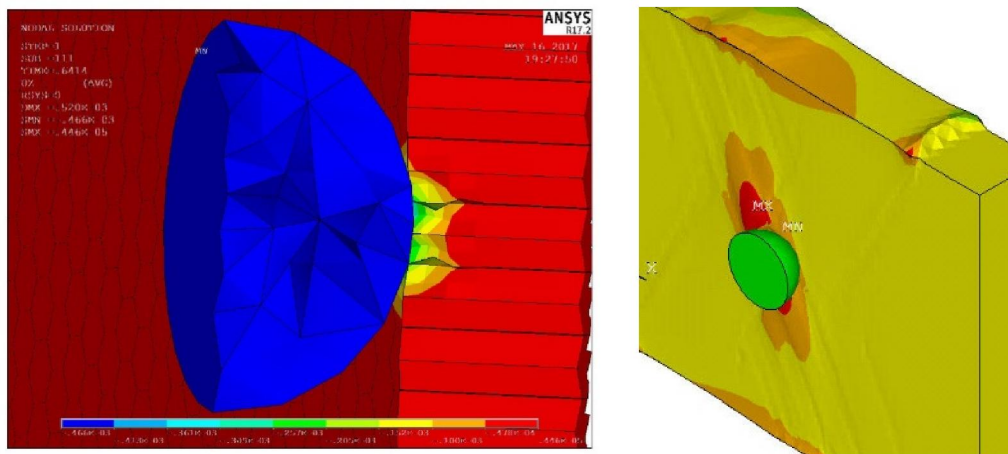
Figure 1.9 Representing response of indentation simulation by surface-to-surface contact elements.

1.3 Material models

Experimental characterization of mechanical properties of all materials incorporated in sandwich panel modelling was extracted experimentally. This include sandwich panel`s skin a carbon fibre reinforced plastic (CFRP) orthotropic material stiffness's and limiting stress/strain values. Adhesive layer physical tests was carried out with the purpose to include in numerical model the plasticity model for bounding layer. A simple coupon tests on tension and compression was carried out to characterize mechanical properties and plastic behaviour of the adhesive material used for assembling CFRP face sheet to honeycomb core. Unipreg CFRP material properties extracted experimetaly are detailed outlined in coupon testing deliverable and average values integrated in FEM are summarised in Table 1.1.

Due to significant adhesive layer thickness, comparable or even exceeded face sheet thickness it was decided to include adhesive layer plasticity into finite element model as bi-linear isotropic hardening material model with experimentally obtained E-modulus (1.97 GPa), yield stress (49 MPa) and tangential modulus (0.01 GPa), Figure 1.10. This assumption are robust enough in case of panel damage propagation due to delamination. Possible damage propagation due delamination/debounding was taken into account by cohesive zone material modelling technique, which realized by the debounding contact algorithm employing maximum debounding normal stress (1.5MPa) and crack propagation energy (575 J/m^2), obtained from experimental drum peel-off tests in combination with bi-linear material model. Cohesive zone material (CZM) model was implemented in shell-

10

RIGA TECHNICAL UNIVERSITY
IMS
INSTITUTE OF MATERIALS AND STRUCTURES

Institute of Materials and Structures
Rīga, Ķīpsalas iela 6A, LV-1048
Tel. +371 67089124
Web. http://www.ims.rtu.lv

solid (reduced) model by the use of contact element interface between honeycomb core and face sheet.

Table 1.1. Unipreg CFRP material properties

Property		Mean values								
		Unipreg 100 g/m²			Unipreg 200 g/m²			Unipreg 200 g/m² (high stiffness)		
E^t, GPa	0°	122.69	115.91	75.52	124.09	122.55	73.33	164.62	164.11	108.37
	90°	8.39	7.79	8.91	6.43	6.63	7.86	-		
E^c, GPa	0°	103.91		102.77	117.60		121.1	-		
	90°	7.70		7.00	7.60		7.84	-		
E^f, GPa		112.83			106.03			-		
G_{12}^{chord}, GPa		6.07		5.78	4.66		4.05	-		
G_{12}, GPa		3.00			3.71			-		
G_{13}, GPa		2.45			2.77			-		
μ	0°	0.33			0.37			0.38		
R^t, MPa	0°	1466			1539			2037		
	90°	46			41			-		
R^c, MPa	0°	481			752			-		
	90°	138			141			-		
τ_{12}^m, MPa		53			50					
R^f, MPa		1427			1217			-		
v_{12}, MPa		207			233			-		
v_{13}, MPa		654			2009			-		

Due to two step analysis procedure – indentation first followed by compression. There was no failure criteria implemented for adhesive material model, in order to avoid excessive stiffness softening in region of indentation caused by failure of material at the tension side of the face sheet, which later was loaded in axial compression. In other words, if failure of adhesive was detected due to indentation of impactor in the face skin. Corresponding elements finite element stiffness was decreased to 0. Nevertheless if and only in case of following pure compressive loading the cracked adhesive layer will sustain (lock down) the compression despite the inhered crack. Thus though eliminated stiffness of delamination affected elements and exclusion from further model analysis the local stiffness at impact region will be decreased.
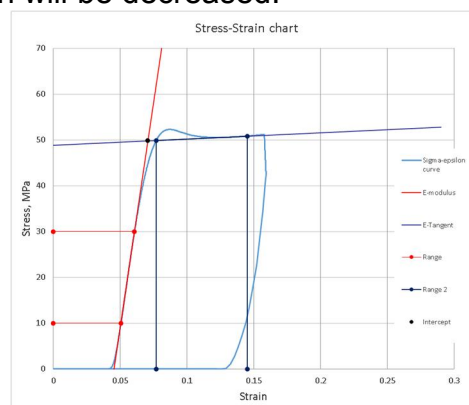
Figure 1.10. Experimental adhesive material characterization.

RIGA TECHNICAL UNIVERSITY
IMS
INSTITUTE OF MATERIALS AND STRUCTURES

Institute of Materials and Structures
Rīga, Ķīpsalas iela 6A, LV-1048
Tel. +371 67089124
Web. http://www.ims.rtu.lv

The characterization of material properties of AL honeycomb core was performed experimentally to determine structural properties used for implementation in reduced finite element model as Hill plasticity rule in combination with bi-linear isotropic hardening plasticity model. Due to significant difference in stiffness of the honeycomb structure for in-plane and out-of-plane axis, Hill plasticity rule with rate of 0.05 for in-plane axis and 1.0 for out-of-plane axis. This was considered in combination with bi-linear isotropic hardening material model. Out-of-plane compressive properties was experimentally characterized by flatwise compression of stabilized honeycomb structure, Figure 1.11. Stress values of honeycomb buckling (3.2 MPa) instead of crushing stress (1.6 MPa), was used in finite element model because of the better indentation depth representation in comparison with experimentally measured indentation depth values.
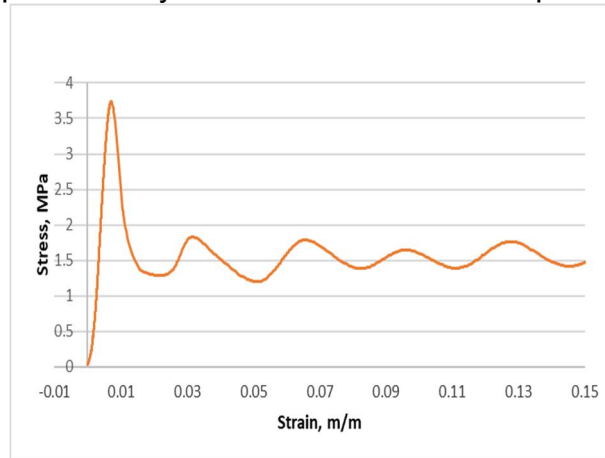
Figure 1.11. Flatwise compression of stabilized honeycomb structure.

1.4 Validation of lamina failure criteria

UD lamina properties obtained during characterization of mechanical properties of UD composite was used as material properties and failure criteria for both finite element models. UD Coupon test simulations with FEM models to validate experimentally obtained failure criteria was carried out for tension and compression of UD specimens with actual cross-section. Comparison was rated in terms of stiffness slope and failure load. Figure 1.12 represents axial tension of UD specimen, and Figure 1.13 represents axial compression of UD specimen. Failure criteria based on Max stress initiation and material stiffness reduction damage evolution law was used for this study [1]. It is obvious that the most satisfied results were obtained for axially loaded specimens, while transversally loaded and shear ($\pm 45^0$) specimens, which are more sensible to damage introduced during specimen manufacturing, was less successive. For axially loaded specimens, especially for tension loaded, there are good correlation was observed in terms of stiffness and breaking load, between experiment and simulation.

RIGA TECHNICAL UNIVERSITY
IMS
INSTITUTE OF MATERIALS AND STRUCTURES

Institute of Materials and Structures
Rīga, Ķīpsalas iela 6A, LV-1048
Tel. +371 67089124
Web. http://www.ims.rtu.lv

873_4_ TENS_0
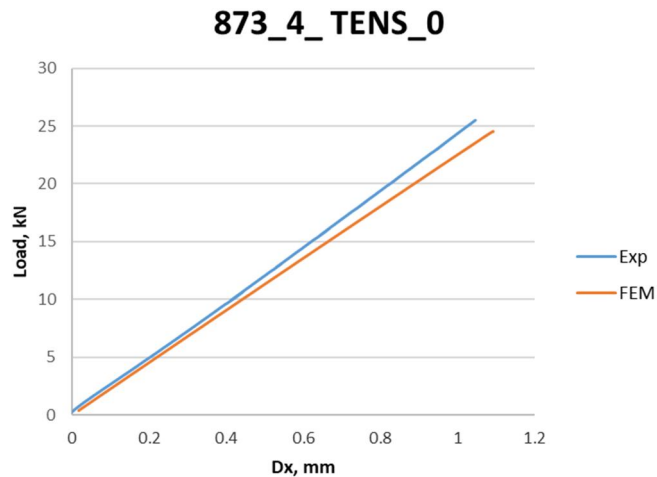
Figure 1.12. Simulation of failure of UD specimen in tension.

874_8_Comp_0
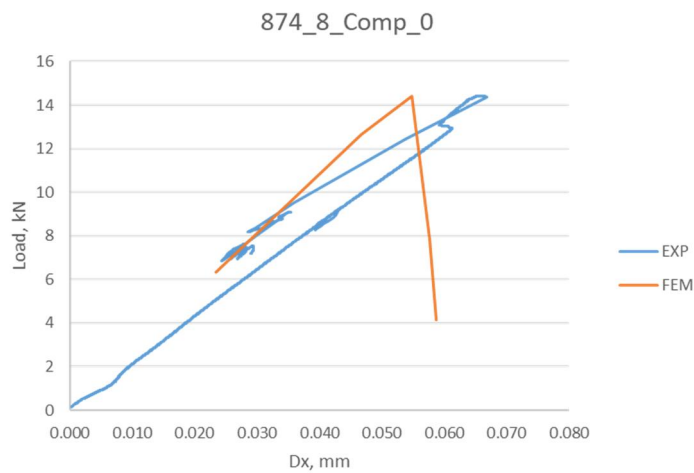
Figure 1.13. Simulation of failure of UD specimen in compression.

1.5 Boundary conditions

Three separate boundary conditions corresponding to certain type of numerical model are addressed. For modal analysis there is no restrains what so ever incorporated in numerical model. On contrary indentation and compression after impact both finite element models share the same boundary conditions. Depending on the loading stage boundary conditions were introduced as simply supportive around perimeter in case of indentation, simulating support of the of indentation frame (restricting translation of the bottom face sheet in direction of indentation (UZ) in combination with fixed individual nodes in the middle of the panel edges to restrict panel of free motion in in-plane direction (UY), which can cause numerical instability and restricting all of the nodes on one of the panel edges (UX). In case of edgewise compressive loading both longitudinal panel edges in depth of 20 mm was clamped, excluding the loading edge where coupled load on node elements where applied.

13

RIGA TECHNICAL UNIVERSITY
IMS
INSTITUTE OF MATERIALS AND STRUCTURES

Institute of Materials and Structures
Rīga, Ķīpsalas iela 6A, LV-1048
Tel. +371 67089124
Web. http://www.ims.rtu.lv

1.6   Mesh sensitivity analyses

Mesh sensitivity analyses was performed with the focus on the most accurate representation of indentation shape and size. Since full 3D finite element model mesh size was dictated by the mesh ability to produce buckling of the honeycomb wall under indenter pressure, at least 2 elements per honeycomb cell side (1.5 mm for 3.2 mm cell) was considered as a minimum desired mesh. Finer mesh was not considered as an option due to high computational costs. As the basis of the finite element mesh for the reduced model was considered the same size as for full 3D model (1.5 mm). Additionally, mesh sensitivity analyses for coarser mesh were performed. Figure 1.14. shows indentation geometry and depth for four different mesh size. It was obvious that the most accurate shape and depth representation was observed for mesh size of 1.5 mm, in terms of shape curvature and indentation depth compared to experimental measurements, carried out by laser sensor. It was observed that for small size indenter (20 mm diameter), indentation depth and area diameter for load of indentation of 500 N, ranges with in: 0.41 - 0.48 mm indentation depth and 16.1 – 18.4 mm indentation area diameter. In other words, 8 mm per indentation wall. That's mean that minimum number of elements needed for accurate indentation shape representation with 8-node shell elements (SHELL281), must be 4, to avoid formation of sharp angle between elements at the tip of the indentation and transition to the flat surface of the panel. Coarse mesh will likely produce diamond shaped indentation with sharp tip or flat shaped indentation with flat tip, thus considerably reducing actual indentation size. Finer mesh densities (less than 1.5 mm) was not considered due to high computational cost.
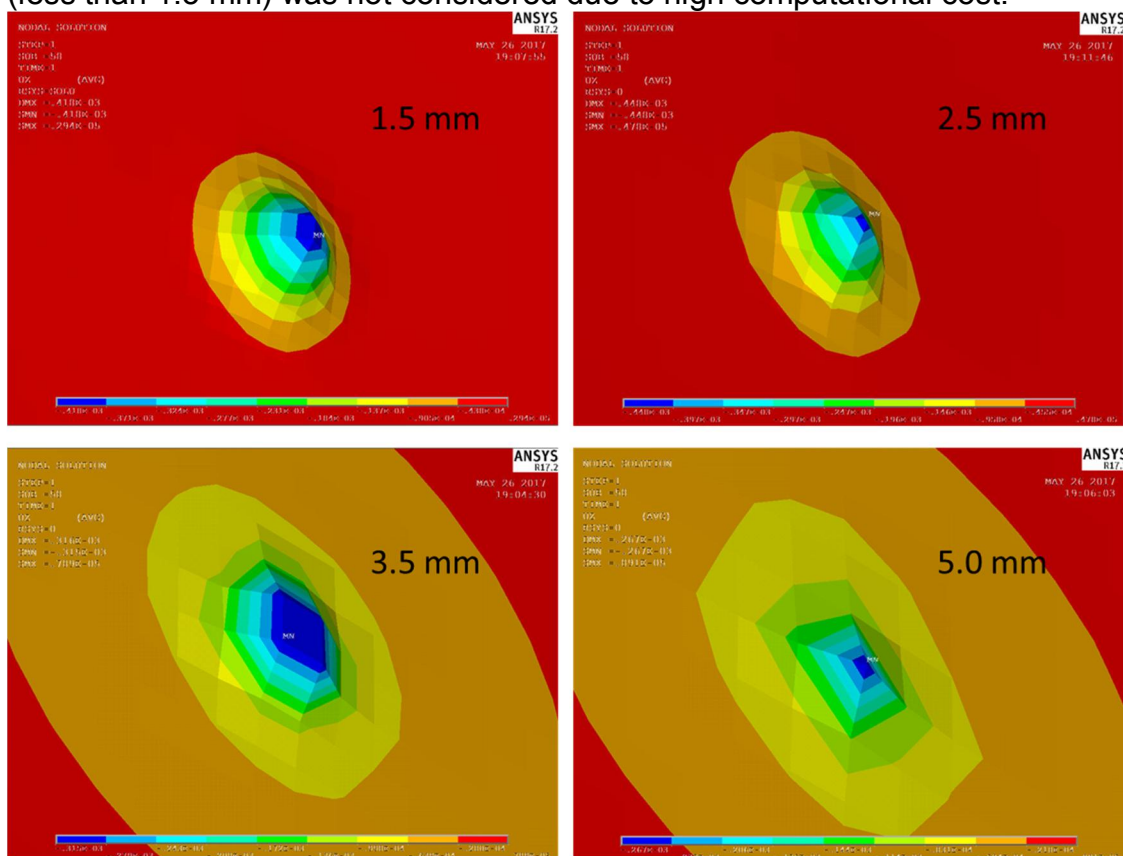
Figure 1.14. Indentation representation for different mesh density.

RIGA TECHNICAL UNIVERSITY
IMS
INSTITUTE OF MATERIALS AND STRUCTURES

Institute of Materials and Structures
Rīga, Ķīpsalas iela 6A, LV-1048
Tel. +371 67089124
Web. http://www.ims.rtu.lv

Figure 1.15., shows dependency of the calculated load carrying capacities depending on selected mesh density. It was seen that despite much lower indentation depth calculated for coarser mesh densities, there was not observed considerable increase in load carrying capacities compared to basic model (1.5 mm). That's mean that despite about 36% lower indentation depth (5 mm mesh density), load carrying capacity increased only by about 4 %, see Table 1.2. Where considerable decrease of depth of indentation observed for coarse mesh, will not produce considerable increase in load carrying capacity, compared to experimental values which are taken as first sign of failure values, which are equivalent to final model failure due to composite damage. It indicates that indentation depth for the current panel configuration was not the key factor for considerable load carrying capacity decreasing.

Table 1.2. Indentation depth and load carrying capacity.

	Indentation depth, mm	Load carrying capacity, kN
Exp.	0.41 - 0.48 (0.44 aver.)	9.854*
1.5 mm	0.418	9.149
2.5 mm	0.448	9.350
3.5 mm	0.315	9.527
5.0 mm	0.267	9.532

* - taking into account first sign of damage

Figure 1.15. Mesh sensitivity analyses.

RIGA TECHNICAL UNIVERSITY
IMS
INSTITUTE OF MATERIALS AND STRUCTURES

Institute of Materials and Structures
Rīga, Ķīpsalas iela 6A, LV-1048
Tel. +371 67089124
Web. http://www.ims.rtu.lv

1.7 Plasticity model sensitivity analyses

Parametric adjustment of four plastic material properties obtained from different sources was performed in the course of development of the reduced finite element model. Plasticity model of the honeycomb core was developed based on early flatwise compression tests, updated flatwise compression test and finally adjustment of plastic properties to match experimentally measured indentation depth. The same way was studied dependency of the plastic properties of the adhesive, used to connect honeycomb core to composite face sheets. Starting with the first values taken from available material data sheets and finalizing with experimentally obtained material properties by coupon tests of adhesive, Table 1.3. Figure 1.16. summarizes different plasticity properties used in calculation. Ecore values varies from 0.457 to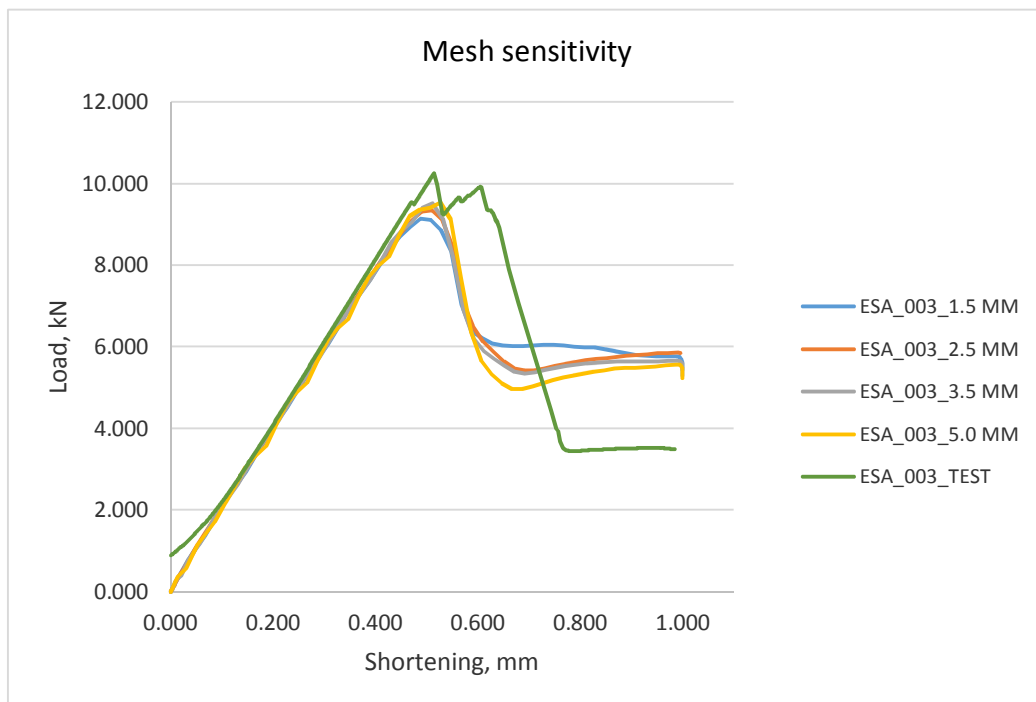 2.35 GPa, with the latest measured value of 0.578 GPa, with the corresponding yield stress of 3.2 MPa, which was adjusted from experimentally obtained plasticity/buckling curve of flatwise honeycomb compression test at which honeycomb buckles at 3.6 MPa and has crushing stress of 1.6 MPa. Final value used for yield stress of honeycomb was 3.2 MPa which produces stiffer response in terms indentation depth at maximum indentation load, but correct residual indentation depth. Crushing stress value recommended in literature [2] for use produces correct indentation depth at maximum indentation load, but overestimates residual indentation depth. Bilinear isotropic hardening rule in combination with Hill plasticity rule was used as a final consideration, to take into account for anisotropy of honeycomb structure.

Adhesive plastic properties were selected as Each = 2.5 MPa based on available datasheet for this material with linear (non-plastic) behaviour, later was replaced by experimentally obtained tension properties of Each = 2.67 GPa with corresponding yield stress 28 MPa, but finally substituted by compressive properties Each = 1.97 GPa with corresponding yield stress 49 MPa. Bilinear isotropic hardening rule was used for all cases. The major criteria for parametric adjustment of plastic properties of honeycomb core and assembling adhesive was stiffness slope which match with the experimental test slope.

Table 1.3. Parametric adjustment of plastic properties.

	ESA_003_clamped	ESA_003_cl_hi =	ESA_003_cl_hi II2	ESA_003_cl_hi II3	ESA_003_cl_hi II4	ESA_003_cl_hi II5	ESA_003_new	ESA_003_new _last	ESA_003_new 2	ESA_003_new 3
Ecore	2.35	2.35 Hill	2.35 Hill	11.12 Hill	0.716 Hill	0.457 Hill	0.578 Hill	0.578 Hill	0.716 Hill	0.716 Hill
yield_core	2.35 MISO	2.35 MISO	2.35 MISO	3.89 BISO	1.6 BISO	1.6 BISO	1.6 BISO	3.2 BISO	3.6 BISO	4 BISO
Eadh	2.5	2.5	2.67	2.67	2.67	2.67	1.97	1.97	1.97	1.97
yield_adh	lin	lin	28 BISO	49 BISO	49 BISO	49 BISO	49 BISO	49 BISO	49 BISO	49 BISO
IND, mm	0.477	0.497	0.57	0.203	0.696	0.688	0.695	0.418	0.388	0.357
Load, kN	10.57	9.471	9.431	8.672	8.889	8.846	8.806	9.149	9.411	9.389

RIGA TECHNICAL UNIVERSITY
IMS
INSTITUTE OF MATERIALS AND STRUCTURES

Institute of Materials and Structures
Rīga, Ķīpsalas iela 6A, LV-1048
Tel. +371 67089124
Web. http://www.ims.rtu.lv
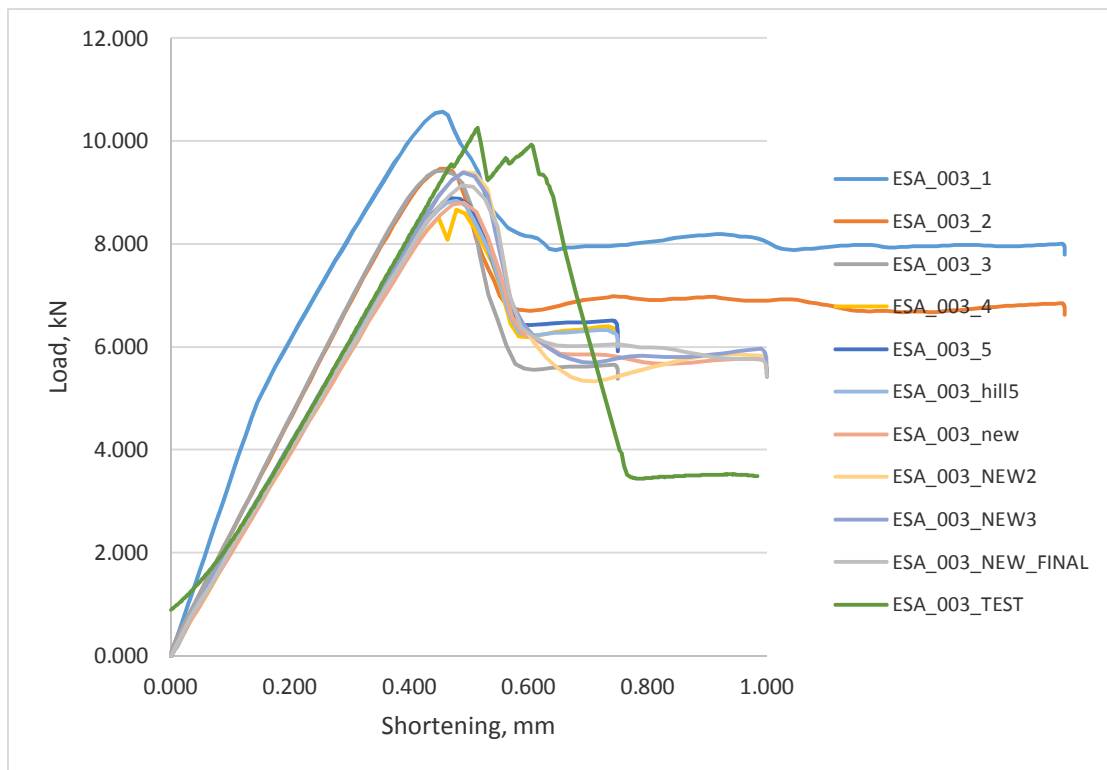
Figure 1.16. Parametric plasticity model adjustment.

RIGA TECHNICAL UNIVERSITY
IMS
INSTITUTE OF MATERIALS AND STRUCTURES

Institute of Materials and Structures
Rīga, Ķīpsalas iela 6A, LV-1048
Tel. +371 67089124
Web. http://www.ims.rtu.lv

2 Verification and validation of numerical approach

2.1 Model verification by modal analysis and self-frequency tests in accordance with ASTM E1876 methodology

A four step procedure have been elaborated based on ASTM E1876 methodology the detailed description was given already in Deliverable 2.1. Summarised verification results are only partial effort, however highlights the principle and main challenges. This methodology provides an equivalent material property identification from physical self-frequency tests and simple weight measurements identifying the mechanical stiffness of tested specimen. It should be noted that methodology is primary developed for beams nevertheless it may be extended and updated for identification of plate stiffness as well. Therefore a dedicated tool for analysis was developed. A flow chart of test procedure is depicted in Figure 2.1.
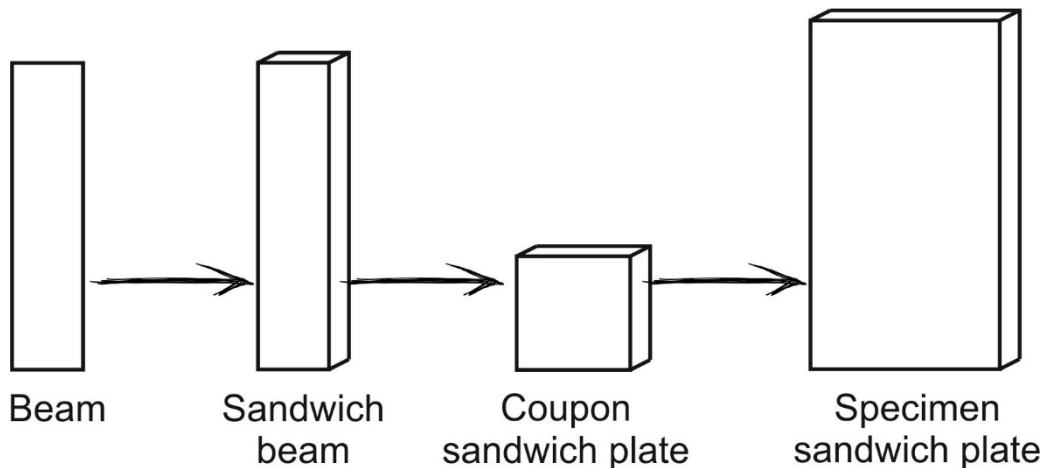
Figure 2.1. Flow chart of verification procedure.

Initially, while mechanical property characterization was expected from WP-4 and only first steps in prototyping was done. Therefore a swift method for identifying realized mechanical properties were required. According to ASTM E 1876 [6] standard the methodology requires – input parameters as m - mass; b – width; l - free span and t – thickness. Furthermore first few natural frequencies f1 and f2, which determine Ex, G and Poisson ratio v. The natural frequencies and vibration modes were scanned using Polytec laser vibrometer (shown in Figure 2.2). For structural excitation a loudspeaker placed 180° opposite the measured area. Measurement conducted in range from 0 to 600 Hz for skin plate and for sandwich beam/panel with "Free Free" boundary conditions (the specimens were hanged to tiny ropes). As there was non-contact measurement and excitation, the additional mass is not considered to influence the physical experiment.

It should be noted that originally method considers isotropic material properties with embedded symmetry thus a special attention identified ortotropic properties should be given to corresponding mode shape – half wave's longitudinal and transverse direction. Both Ex and Ey could be identified along with Gxy. It should be noted that Poison ratio showed no sensitivity and was neglected. Initial procedure

18

RIGA TECHNICAL UNIVERSITY
IMS
INSTITUTE OF MATERIALS AND STRUCTURES

Institute of Materials and Structures
Rīga, Ķīpsalas iela 6A, LV-1048
Tel. +371 67089124
Web. http://www.ims.rtu.lv

include verification of different scale specimens, however finally actual size prototype panels where modelled produced according to required technical excellence.

Initial four sandwich panels was manufactured and delivered for identification purposes Table 2.1. They been labelled ESA_001, ESA_002, ESA_003, and ESA_004.

Table 2.1. Dimension of in initial four panel series

| SP name | Geometry | | | | |
	Length, mm	Width, mm	Thickness, mm	Mass, g	Density, kg/m³
ESA 001			11.28	237.1	217.6
ESA 002	460	210	11.27	240.2	220.7
ESA 003			11.14	225.7	209.7
ESA 004			11.11	221.0	205.9

The special attention was given for verification of proper scale panel FEM mesh size correlation. The convergence of the element mesh size is presented in

Table 2.2. Comparison of real and calculated values is shown in Table 2.3.

Table 2.2. Convergence of finite element mesh size

Frequency, Hz (m; n)	Elements size, 2 mm	Elements size, 3 mm	Elements size, 4 mm
1 (0; 2)	320.13	320.15	320.98
2 (1; 1)	405.97	406.01	406.98
3 (1; 2)	868.99	869.02	871.62
4 (0; 3)	870.23	870.30	872.66
5 (2; 0)	1439.8	1439.9	1443.5
6 (1; 3)	1455.0	1455.5	1460.3
7 (2; 1)	1634.0	1634.5	1639.6
8 (0; 4)	1693.3	1693.5	1698.2

Table 2.3. Comparison of experimental frequencies and waveforms with frequencies from ANSYS

A frequency response among initial four panels are summarized in Figure 2.2. A mesh sensitivity of shell only solid only and reduced – shell solid FEM models are outlined in Figure 2.3. Basically shell only and shell solid models are robust and mesh size are relatively not affecting modal response.

RIGA TECHNICAL UNIVERSITY
IMS
INSTITUTE OF MATERIALS AND STRUCTURES

Institute of Materials and Structures
Rīga, Ķīpsalas iela 6A, LV-1048
Tel. +371 67089124
Web. http://www.ims.rtu.lv
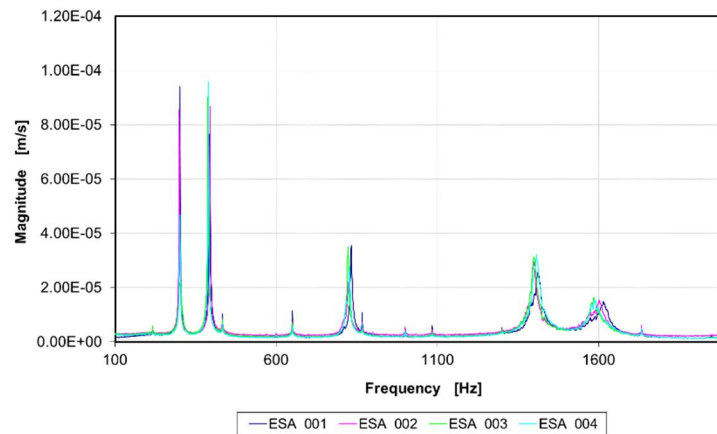
Figure 2.2. Eigen frequency response of initial panel samples.

f Hz (m; n)	EXP		FEM		Δ, %
1 (0; 2)	301.25		320.15		-6.27
2 (1; 1)	393.13		406.01		-3.28
3 (1; 2)	811.25		869.02		-7.12
4 (0; 3)	832.50		870.30		-4.54
5 (2; 0)	1388.75		1439.9		-3.68
6 (1; 3)	1410.63		1455.5		-3.18
7 (2; 1)	1573.75		1634.5		-3.86
8 (0; 4)	1615.00		1693.5		-4.86

RIGA TECHNICAL UNIVERSITY

IMS

INSTITUTE OF MATERIALS AND STRUCTURES

Institute of Materials and Structures
Rīga, Ķīpsalas iela 6A, LV-1048
Tel. +371 67089124
Web. http://www.ims.rtu.lv
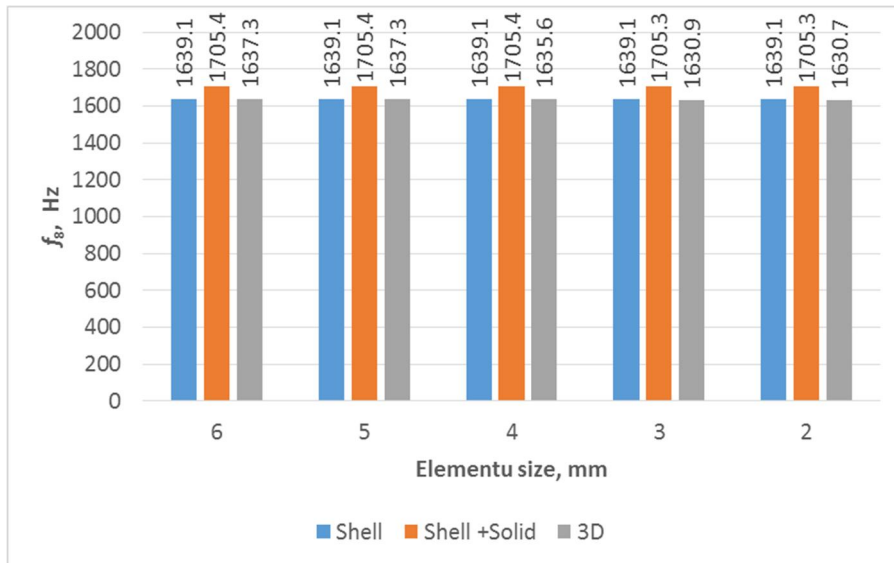
Figure 2.3. Verification of material properties.

2.2 Verification of considered damage types

In order to assess the damage sensitivity three types of indentation were considered for evaluation: artificial HC depression and artificial debounding, as well as, mechanical indentation of the assembled panel. Artificial debounding of the face sheet was considered as one of the possible hidden hardly detectable defects, caused by improper manufacturing/curing process. In the current study artificial debounding was realized by two different approaches. The first was mechanical indentation (depression) of the honeycomb structure with four different diameter circular flat indenters (12, 20, 30, 50 mm) to the depth of about 1 mm to guarantee debounding of the face sheet in this region, Figure 2.4. The only drawback of this type of imperfection was the fact that honeycomb in the region of indentation was stiffened by plastically deformed cell part, i.e. additional stiffness and space for face sheet to buckle was created.

The second type of artificial indentations was absence of adhesive layer between honeycomb and face sheet for three different diameter spots (20, 35, 48 mm), Figure 2.5.

RIGA TECHNICAL UNIVERSITY
IMS
INSTITUTE OF MATERIALS AND STRUCTURES

Institute of Materials and Structures
Rīga, Ķīpsalas iela 6A, LV-1048
Tel. +371 67089124
Web. http://www.ims.rtu.lv
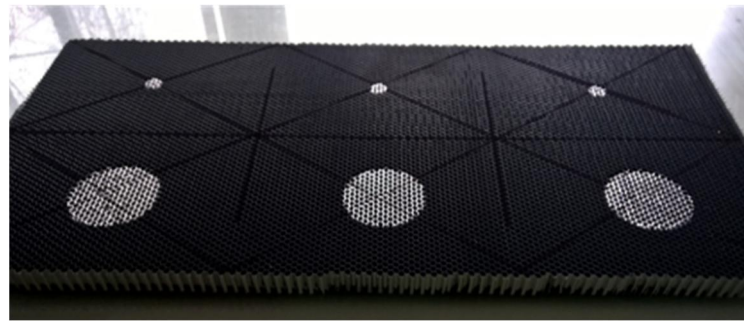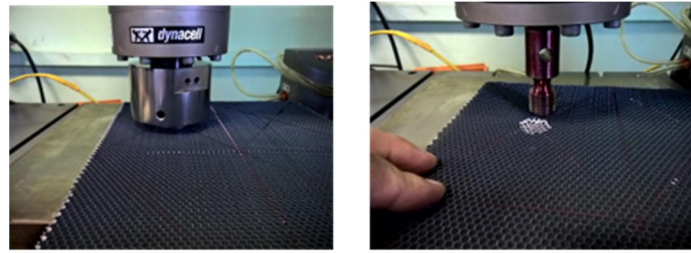
Figure 2.4. Artificial honeycomb indentation defects.

Figure 2.5. Artificial debounding (absence of adhesive layer).

In both cases it should be noted that only largest deboundings can be classified as barely visible damage, otherwise they are not visible at all and hidden beneath the outer surface. Experimental compression tests for those panels showed that only comparatively large debounding will affects compressive load carrying capacity, compared to unaffected panel of the same composition, Figure 2.6.
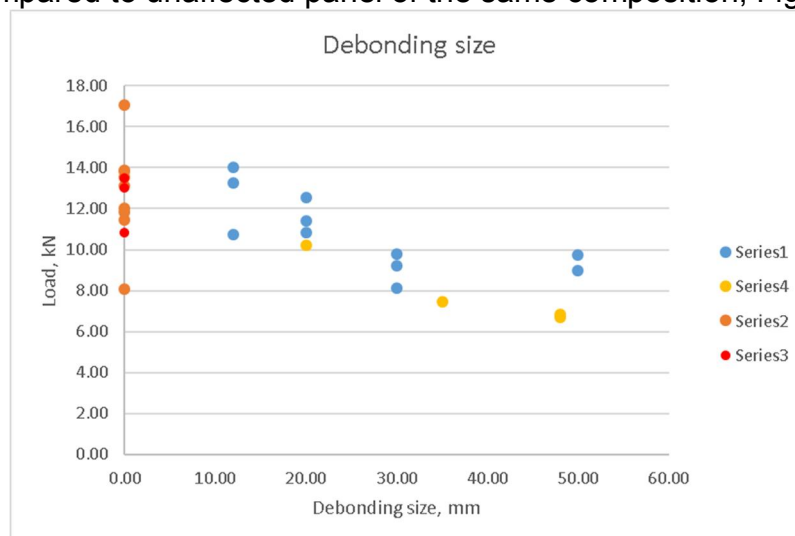
Figure 2.6. CAI load carrying capacity depending on debounding size.

RIGA TECHNICAL UNIVERSITY
IMS
INSTITUTE OF MATERIALS AND STRUCTURES

Institute of Materials and Structures
Rīga, Ķīpsalas iela 6A, LV-1048
Tel. +371 67089124
Web. http://www.ims.rtu.lv

While the first two debounding damage scenarios can be addressed to panel manufacturing faults, the third indentation type can be addressed to improper already assembled panel handling. The third indentation type considered was indentation by stiff (spherical) object. Indentation was introduced by steel spherical indenter by quasi-static loading with careful load control and instrumented indentation depth measurement. Indentation was performed on standard indentation frame for 150 x 100 mm panels, with 12.5 mm support width on all the edges.

2.3   Verification of indentation numerical model

Identification FEM model validation in terms of indentation depth and shape was compared to experimentally tested - laser scanned residual dent shape of the panel surface after indentation. Finite element model simulation of indentation confirmed good agreement with scanned panels. More than dozen results have been analysed and already uploaded on projects homepage (Bnm4eks.rtu.lv) under section of design tools. A screen shot taken from project web page preliminary tool are shown in Figure 2.7. shows as well as, results were compared to analytically calculated indentation depth values based on ASTM D7766 and D7139 [5-6].

Figure 2.7. A screen shot from preliminary design tool available at bnm4eks.rtu.lv.

RIGA TECHNICAL UNIVERSITY
IMS
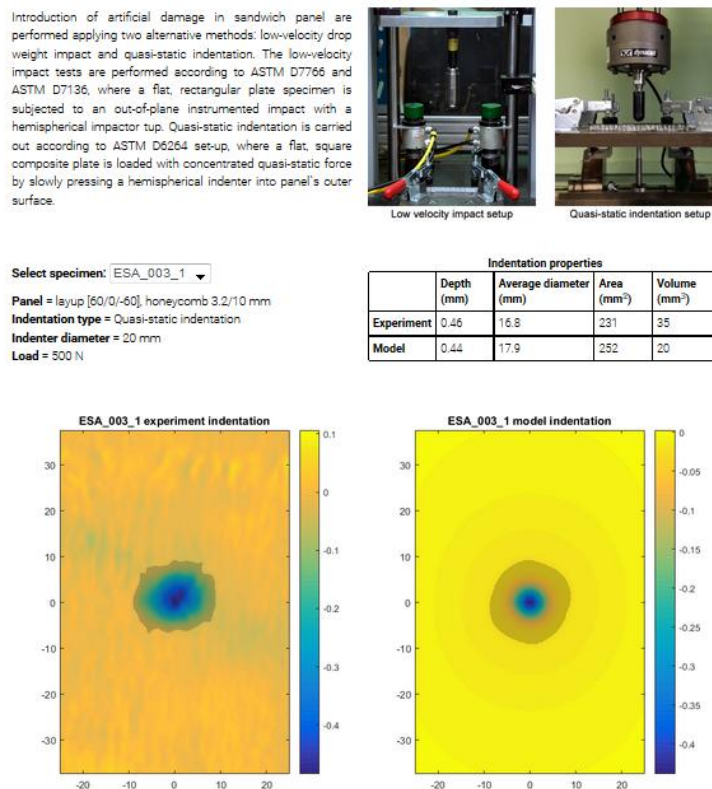INSTITUTE OF MATERIALS AND STRUCTURES

Institute of Materials and Structures
Rīga, Ķīpsalas iela 6A, LV-1048
Tel. +371 67089124
Web. http://www.ims.rtu.lv
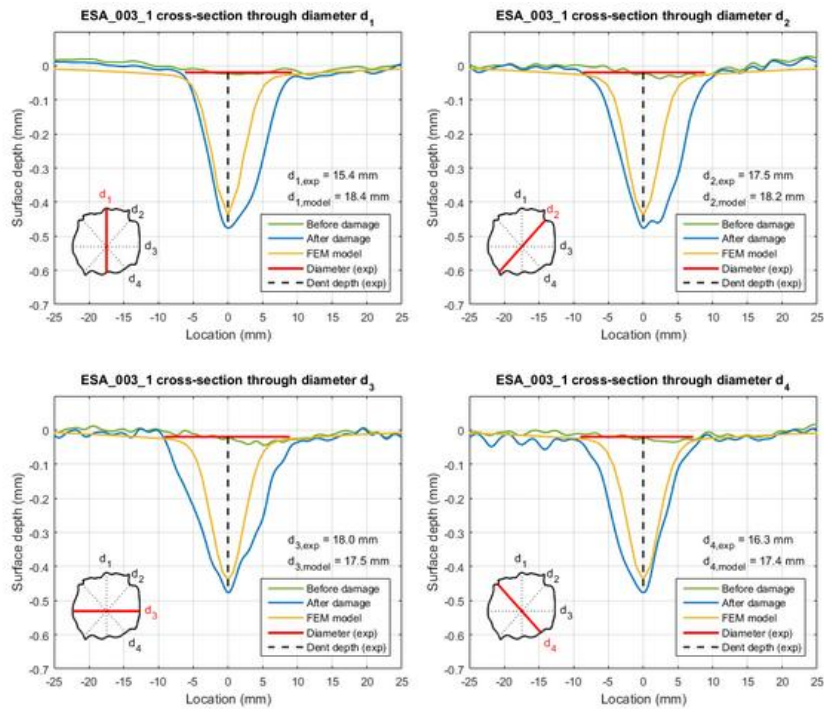
Figure 2.8. A validation between numerical and experimental indentation depth estimation a whole test data set is available on bnm4eks.rtu.lv.

It should be noted that numerical models are based on averaged parameters (such as: ply thickness, adhesive thickness, CFRP material props, etc.), which with the certain degree differs to those found in individual panels. This can lead to deference of indentation depth for individual panels, in terms of direct comparison to FEM model results. Comparison of the depth of indentation calculated for both numerical model showed good correlation in terms of depth, despite much higher numerical effort needed for full model to obtain solution. This was the reason of creation of simplified reduced model. Additionally, direct extraction of desired material properties for core structure by experimental tests has more benefits than calculation of full model with material properties of unknown source.

2.3.1 Validation of FEM model based on CAI experiments

Validation of CAI experiments with finite element model (reduced model only) showed good agreement of results in terms of stiffness, Figure 2.9. Obtained peak in load carrying capacity of numerical models shows lower values than experimental, however in many cases experimental specimens showed gradual damage propagation in form of non-significant load drops caused by face sheet delamination's or permanent damage accumulation, which probably not leading to permanent stiffness reduction, like it was identified by finite element model.

RIGA TECHNICAL UNIVERSITY
IMS
INSTITUTE OF MATERIALS AND STRUCTURES

Institute of Materials and Structures
Rīga, Ķīpsalas iela 6A, LV-1048
Tel. +371 67089124
Web. http://www.ims.rtu.lv
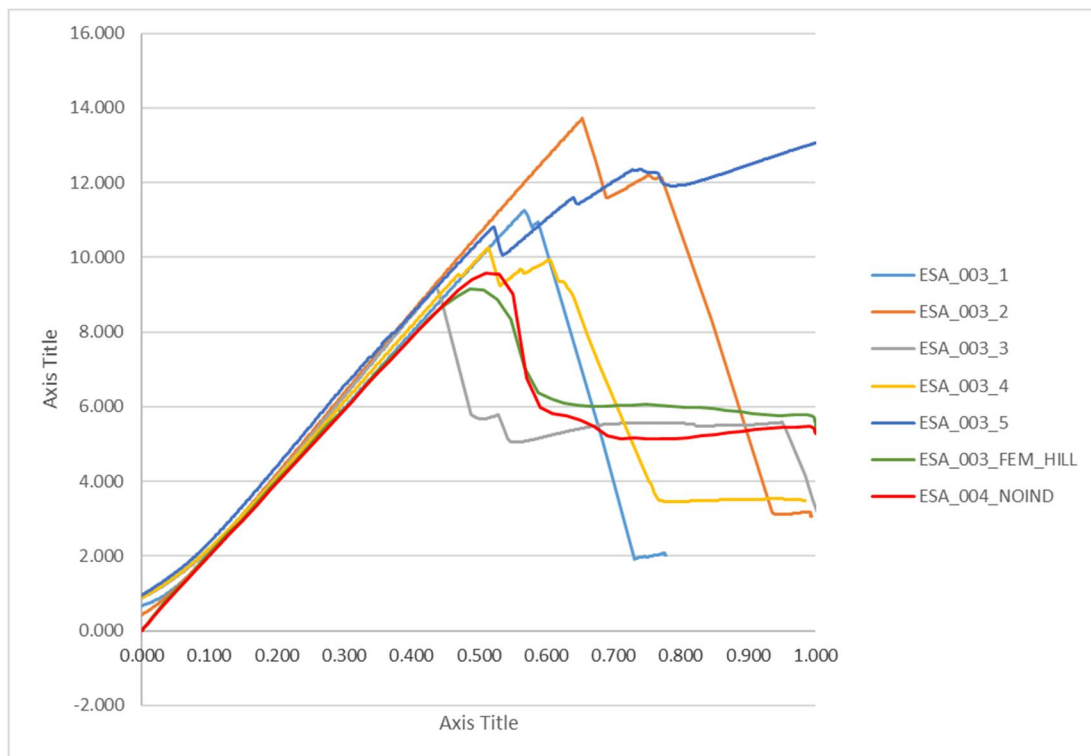
Figure 2.9. ESA_003 series compression experimental curves.

It should be noted that for the present experimental study panels having significant honeycomb stiffness in transverse direction are not sensitive to side impact imperfections and as it was seen on Figure 2.10., for experimental tests of ESA_009 and ESA_010 series (ESA_010 without impact), barely visible damage for the current set of materials was not significant for the load carrying capacity. Scatter of maximum load carrying capacities indicates that there are different key factors that affect load values for individual specimens within series. For the broad majority of tested specimens damage initiation was not related with indentation, but rather edge effects (damage propagation initiated at the free edges), Figure 2.11. Honeycomb height was not the factor affecting load carrying capacity, rather face sheet lay-up, Figure 2.12.

RIGA TECHNICAL UNIVERSITY
IMS
INSTITUTE OF MATERIALS AND STRUCTURES

Institute of Materials and Structures
Rīga, Ķīpsalas iela 6A, LV-1048
Tel. +371 67089124
Web. http://www.ims.rtu.lv

Figure 2.10. ESA_009 & ESA_010 series CAI experimental curves.
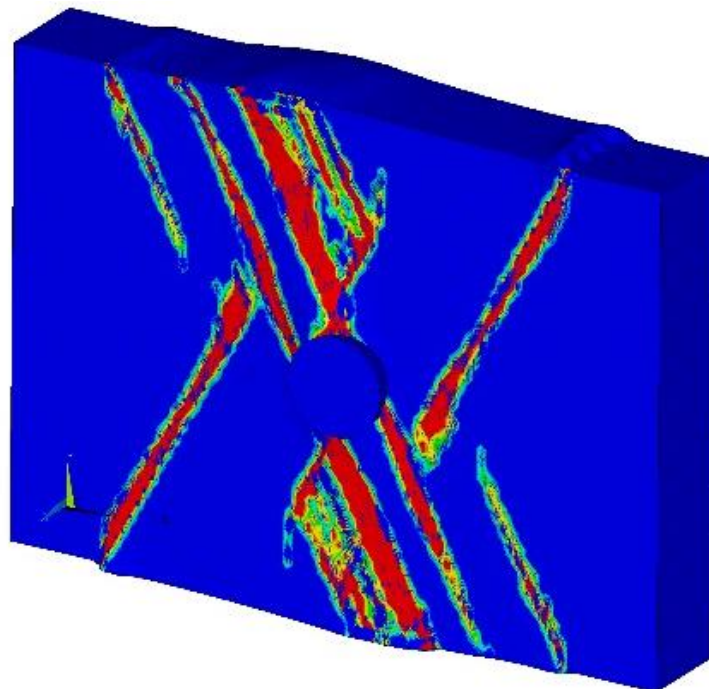
Figure 2.11. Composite fibre failure mode according to Max stress criteria.

RIGA TECHNICAL UNIVERSITY
IMS
INSTITUTE OF MATERIALS AND STRUCTURES

Institute of Materials and Structures
Rīga, Ķīpsalas iela 6A, LV-1048
Tel. +371 67089124
Web. http://www.ims.rtu.lv
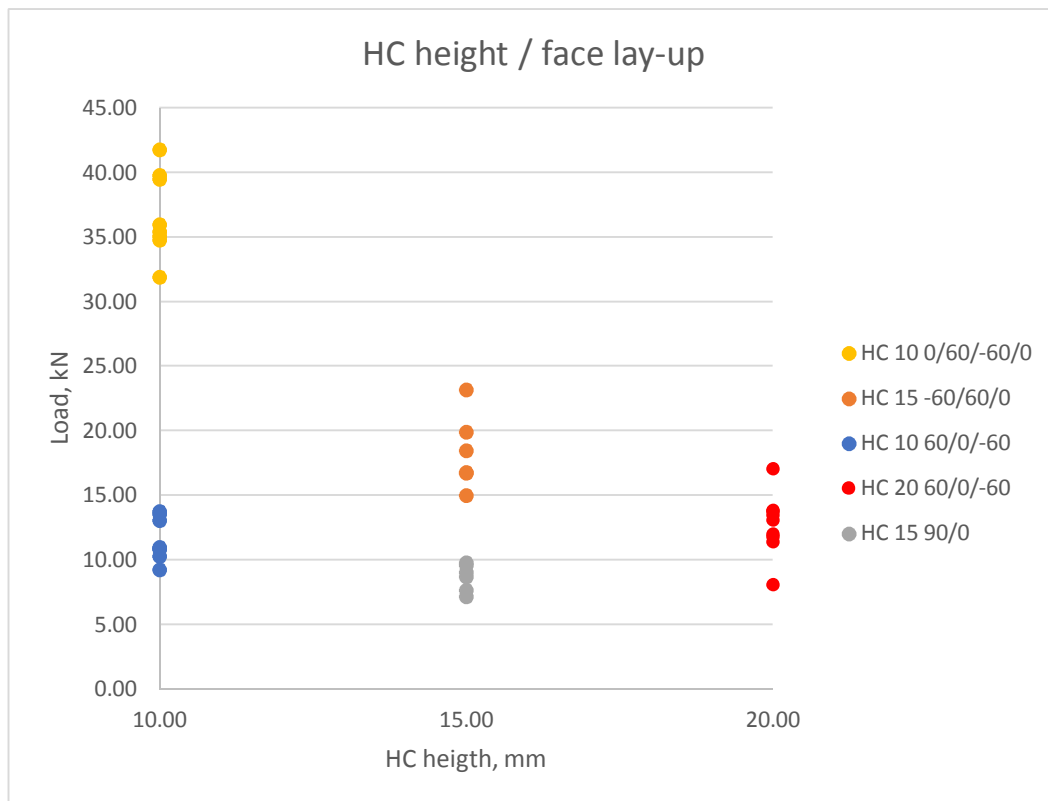
Figure 2.12. Load carrying capacity depending on lay-up and honeycomb height.

2.4 Numerical model validation with tested panels
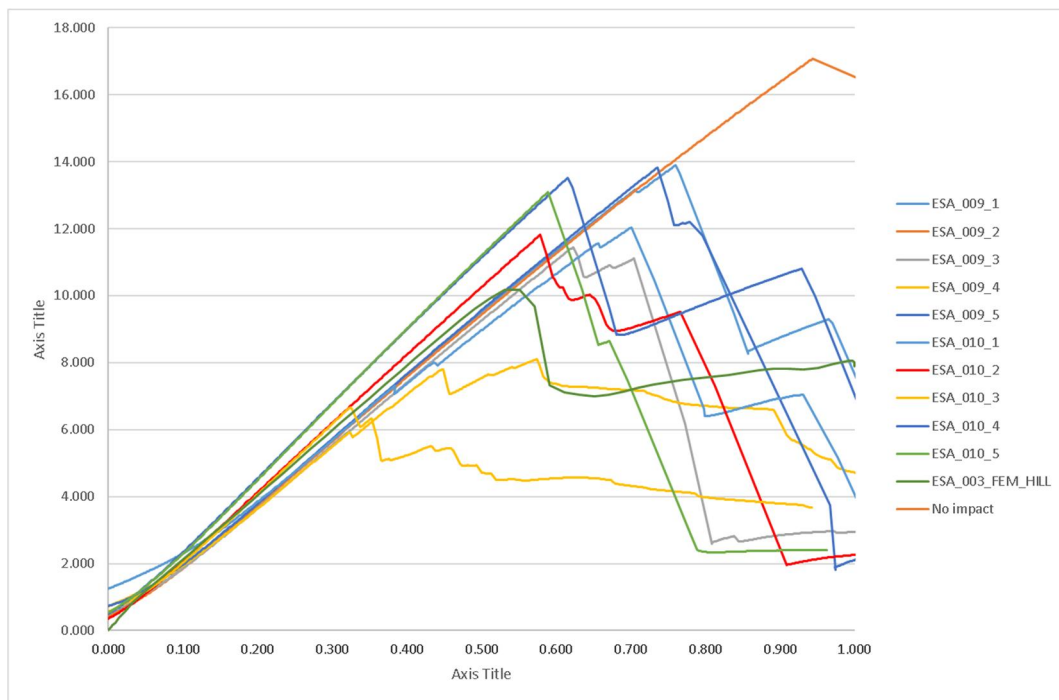
Experimental compression after impact (CAI) tests on panels with different lay-ups were carried out. Four different lay-up configurations was considered with the aim of to find relationship between load carrying capacity and lay-up ply count, lay-up ply orientation order and honeycomb height.

All performed experimental tests (about 50), were performed after quasi-static indentation of 20 mm diameter indenter with the indentation force of 500 N. Figure 2.13., shows that additional face sheet lay-up layer will produce considerable increase in load carrying capacity (about 50% for 0/60/-60/0 vs. -60/60/0). The same can be addressed to dropping off one layer (-60/60/0 vs. 90/0). Positioning of outside layer with 0 orientation (loading direction) compared to -60/0/60, will slightly increase the load carrying capacity (about 30%). There is no evidence of any dependency of the honeycomb height if we compare specimens with the same lay-up (-60/0/60), but different height of honeycomb. The height of the honeycomb structure has less significant or even no impact on depth of indentation, in contrast to face sheet ply count.

RIGA TECHNICAL UNIVERSITY
IMS
INSTITUTE OF MATERIALS AND STRUCTURES

Institute of Materials and Structures
Rīga, Ķīpsalas iela 6A, LV-1048
Tel. +371 67089124
Web. http://www.ims.rtu.lv
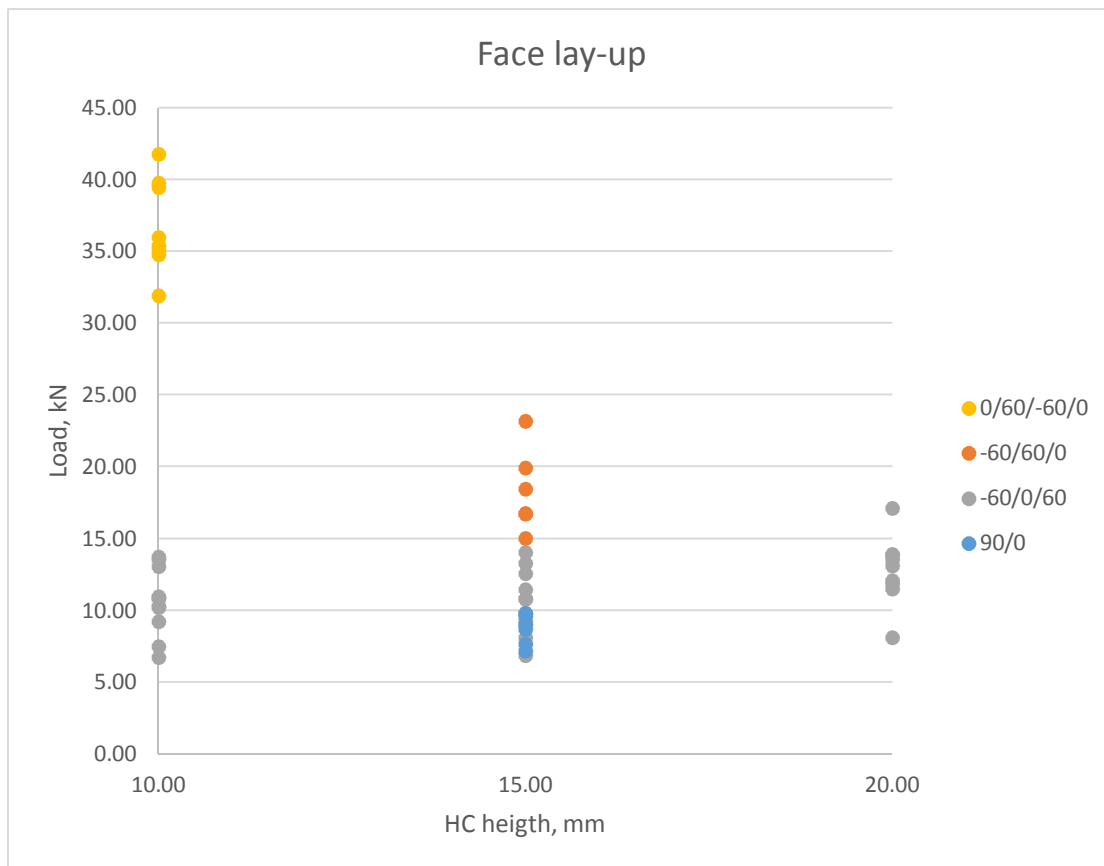
Figure 2.13. Tested panels with different lay-ups.

Figure 2.13., shows dependency of the ply count on the load carrying capacity, regardless lay-up, as well as, range of experimental data for each group. 4-ply load carrying capacity range within two series of similar specimens (cut from two equal panels), showed very low sensitivity to introduced imperfections, i.e. there are no difference between damaged and non-damaged specimens. 3-ply series has broader discrepancy due to different lay-ups, but have similar tendency to be less sensible to introduced imperfections. 2-ply series showed the same load carrying capacity values as lower end 3-ply series Figure 2.14., indicating that panels regardless different lay-ups can reach plato of composite damage regardless of original lay-up. It should be noted that increase in face sheet lay-up thickness will more likely lead to composite crush / failure, while softer 2-ply face sheets will encourage face sheet delamination propagation damage mechanism.

RIGA TECHNICAL UNIVERSITY
IMS
INSTITUTE OF MATERIALS AND STRUCTURES

Institute of Materials and Structures
Rīga, Ķīpsalas iela 6A, LV-1048
Tel. +371 67089124
Web. http://www.ims.rtu.lv
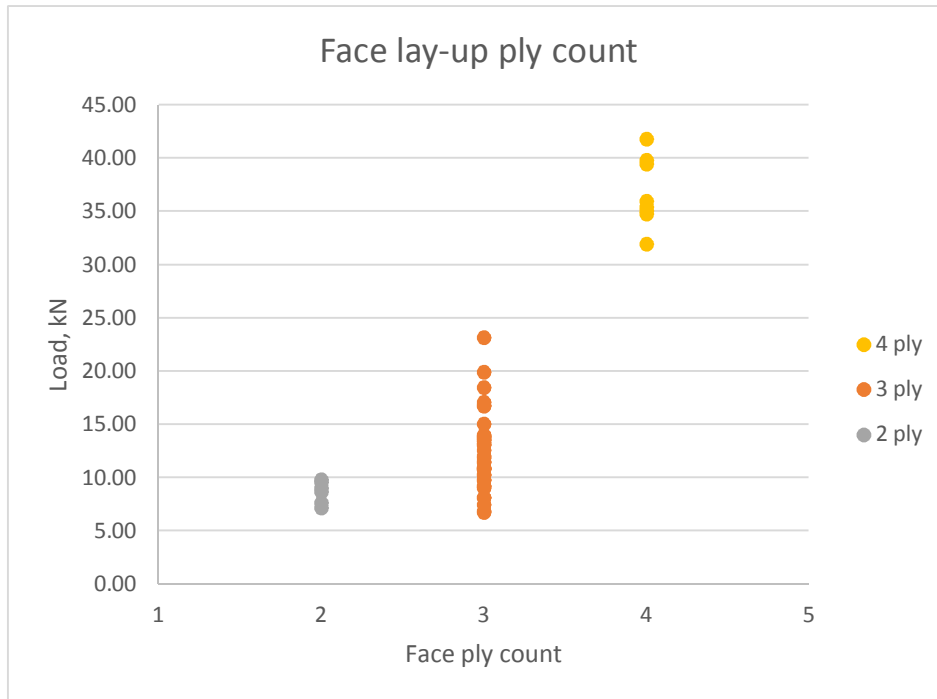
Figure 2.14. Face lay-up ply count.

3 Analytical model of residual indentation upon low-velocity impact of a sandwich panel

A characteristic mode of BVID in aluminium honeycomb core/CFRP face sheet sandwich structure is a dent left by the impactor, which is formed due to crushing and/or plastic deformation of the core. Such a residual indentation of a face sheet affects adversely the CAI strength of the sandwich by serving as a geometrical imperfection initiating inwards buckling of the face sheet and as a stress concentrator initiating face sheet fracture, see e.g. [7-10]. In either case, the reduction in CAI strength is directly related to the size and shape of the dent. Hence, an analytical tool for prediction of the residual dent geometry based on mechanical and geometrical characteristics of the sandwich and the impactor parameters would apparently be useful in, e.g., early design stages of a sandwich structure.

The existing analytical models of low-velocity impact or quasi-static indentation applicable to Al honeycomb core/CFRP face sheet sandwich panels are focused primarily on the active loading, seeking to estimate maximum force and energy dissipated during impact [10-17], but largely disregarding the residual indentation and its geometry. In the present work, an analytical model for quasi-static indentation of a sandwich panel by a hemispherical indenter [12] is refined, extended to prediction of the geometry of residual dent, and validated against experimental data of Al honeycomb/CFRP sandwich panels.

RIGA TECHNICAL UNIVERSITY
IMS
INSTITUTE OF MATERIALS AND STRUCTURES

Institute of Materials and Structures
Rīga, Ķīpsalas iela 6A, LV-1048
Tel. +371 67089124
Web. http://www.ims.rtu.lv

3.1 Load-indentation response

Consider quasi-static indentation of a rigidly supported composite sandwich by a rigid indenter, perpendicular to the facesheet surface, with a hemispherical tip of radius R. The geometrical model of face sheet displacement and the contact surface shown in Figure 3.1. is based on that proposed in [12]: the surface S_1 corresponds to frictionless contact zone between the indenter and the face sheet, extending radially $0 \leq r \leq \rho$, where r is the radial coordinate of the polar coordinate system with origin at the axis of the intender. S_2 designates free surface of the face sheet experiencing deflection due to indentation and extending within $\rho \leq r \leq a$, where a is the radius of indentation zone.

Neglecting the possible effect of the face sheet lay-up on geometry of the indentation, we assume that the dent is axially symmetric and deflection of the face sheet is function o the radial co-ordinate only, $w = w(r)$. The respective analytical expression for deflection is given by Eq. (3.1). Within the contact zone S_1, $w(r)$ follows the geometry of the tip of the rigid indenter as in [12]; displacement of the tip of indenter with respect to the unperturbed surface of the face sheet is denoted by δ. The shape of deflection within zone S_2 is assumed such that $w(r)$ and $w'(r)$ are continuous at $r = \rho$ and deflection vanishes at $r = \rho$ smoothly, i.e. both $w(a) = 0$ and $w'(a) = 0$. Thus, refining the geometrical model of [12], we have hereby assumed a strictly axially symmetric deflection with $w = w(r)$ also in zone S_2.
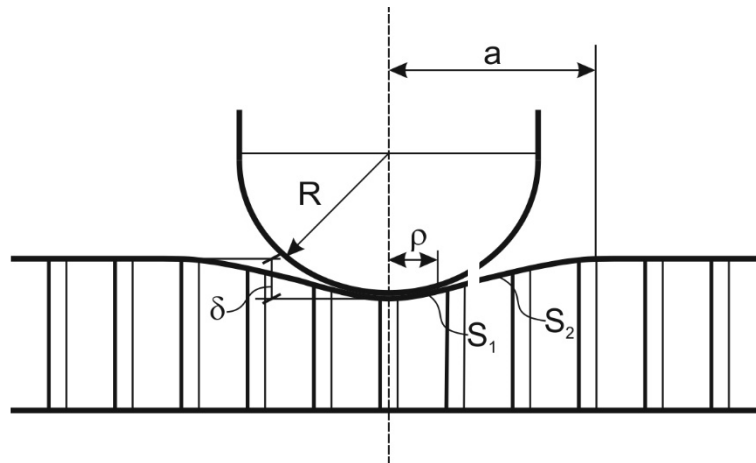

Figure 3.1. Schematic of indentation geometry.

$$w(r) = \begin{cases} \sqrt{R^2 - r^2} + \delta - R & 0 \leq r \leq \rho \\ \left(\sqrt{R^2 - \rho^2} + \delta - R \right)\left(1 - \frac{r - \rho}{a - \rho} \right)^2 & \rho \leq r \leq a \end{cases} \qquad (3.1)$$

Continuity of the first derivative of $w(r)$, given by Eq. (3.1), at $r = \rho$ yields a constraint

RIGA TECHNICAL UNIVERSITY
IMS
INSTITUTE OF MATERIALS AND STRUCTURES

Institute of Materials and Structures
Rīga, Ķīpsalas iela 6A, LV-1048
Tel. +371 67089124
Web. http://www.ims.rtu.lv

$$\frac{\rho(a-\rho)}{2\sqrt{R^2-\rho^2}} = \sqrt{R^2-\rho^2} + \delta - R. \tag{3.2}$$

The total potential energy Π of the system schematically presented in Fig. 3.1 is

$$\Pi = U + D - W \tag{3.3}$$

where U stands for the elastic energy of the system, D denotes dissipated energy, and W is the work of external forces. The latter, for a given indentation force P and indenter displacement δ, is

$$W = P\delta \tag{3.4}$$

Appearance of the BVID implies that maximum displacement of the sandwich face sheet should exceed considerably its thickness. Then U can be approximated by the elastic energy of the face sheet treated as a membrane, and D – by the work dissipated by plastic crushing of the core.

Areal strain energy density u of the face sheet in its axes of orthotropy is

$$u = \frac{1}{2}\left(A_{11}\varepsilon_{11}^2 + 2A_{12}\varepsilon_{11}\varepsilon_{22} + A_{22}\varepsilon_{22}^2 + A_{66}\varepsilon_{66}^2\right) \tag{3.5}$$

where A_{ij} are components of the stiffness matrix of the face sheet and ε_{ij} are the respective membrane strains. They are expressed via the face sheet deflection $w(r)$ as follows (see e.g. [177])

$$\varepsilon_{11} = \frac{1}{2}\left(\frac{\partial w}{\partial r}\cos\varphi\right)^2$$

$$\varepsilon_{22} = \frac{1}{2}\left(\frac{\partial w}{\partial r}\sin\varphi\right)^2 \tag{3.6}$$

$$\varepsilon_{66} = \frac{1}{2}\left(\frac{\partial w}{\partial r}\right)^2 \sin 2\varphi$$

where φ is the angular coordinate in the polar coordinate system. Substituting Eqs. (3.1), (3.6) in Eq. (3.5) and integrating the latter in polar coordinates over zone S_1, strain energy U_1 of the face sheet below the indenter is obtained as follows

$$U_1 = \int_0^\rho \int_0^{2\pi} u\, r\, d\varphi dr = \frac{\pi L}{64}\left[\frac{R^2\rho^2}{R^2-\rho^2} + \rho^2 + 2R^2 \log\left(1 - \frac{\rho^2}{R^2}\right)\right] \tag{3.7}$$

where $L = 3A_{11} + 2A_{12} + 3A_{22} + 4A_{66}$. In the same way, strain energy U_2 of the face sheet beyond the contact surface, within zone S_2, is evaluated

31

RIGA TECHNICAL UNIVERSITY

IMS

INSTITUTE OF MATERIALS AND STRUCTURES

Institute of Materials and Structures
Rīga, Ķīpsalas iela 6A, LV-1048
Tel. +371 67089124
Web. http://www.ims.rtu.lv

$$U_2 = \int\limits_{\rho}^{a}\int\limits_{0}^{2\pi} u\, r\, d\varphi dr = \frac{\pi L}{60} \frac{(a+5\rho)\left(\sqrt{R^2-\rho^2}+\delta-R\right)^4}{(a-\rho)^3}.$$

(3.8)

Deformation behaviour of the honeycomb core in flatwise compression is assumed to be rigid-perfectly plastic with the yield limit equal to the crushing stress q of the core, as demonstrated to be sufficiently accurate by the previous research [10-16]. Then the energy dissipated by core crushing below the indenter, D_1, and beyond it, D_2, is estimated, respectively, as

$$D_1 = \int\limits_{0}^{\rho}\int\limits_{0}^{2\pi} q\, w\, r\, d\varphi dr = \frac{\pi q}{3}\left[2R^3 - 3(R-\delta)\rho^2 - 2(R^2-\rho^2)^{3/2}\right]$$

(3.9)

and

$$D_2 = \int\limits_{\rho}^{a}\int\limits_{0}^{2\pi} q\, w\, r\, d\varphi dr = \frac{\pi q}{6}(a-\rho)(a+3\rho)\left(\sqrt{R^2-\rho^2}+\delta-R\right).$$

(3.10)

It follows from the derivations above that the potential energy Eq. (3.3) takes the form

$$\Pi = U_1 + U_2 + D_1 + D_2 - W.$$

(3.11)

Due to the geometrical constraint Eq. (3.2), only two of the quantities ρ, δ, a are independent. Expressing a from Eq. (3.2)

$$a = \rho + \frac{2}{\rho}\left(R^2 - \rho^2 - (R-\delta)\sqrt{R^2-\rho^2}\right)$$

(3.12)

and substituting Eq. (3.12) into Eqs. (3.7)-(3.10), we finally obtain the potential energy Eq. (3.11) as $\Pi = \Pi(\delta,\rho)$:

$$\Pi(\delta,\rho) = -P\delta + \frac{1}{64}\pi L\left(\frac{R^2\rho^2}{R^2-\rho^2} + \rho^2 + 2R^2\log\left(1-\frac{\rho^2}{R^2}\right)\right) +$$

$$\frac{1}{240}\pi L\frac{\rho^2\left(\sqrt{R^2-\rho^2}-R+\delta\right)^4\left(R^2+2\rho^2-(R-\delta)\sqrt{R^2-\rho^2}\right)}{\left(R^2-\rho^2-(R-\delta)\sqrt{R^2-\rho^2}\right)^3} +$$

$$\frac{1}{3}\pi q\left(2R^3 - 3(R-\delta)\rho^2 - 2(R^2-\rho^2)^{3/2}\right) +$$

$$\frac{2}{3}\pi q\frac{\left(\left(R^2-(R-\delta)\sqrt{R^2-\rho^2}\right)^2 - \rho^4\right)\left(\sqrt{R^2-\rho^2}-R+\delta\right)}{\rho^2}$$

(3.13)

RIGA TECHNICAL UNIVERSITY
IMS
INSTITUTE OF MATERIALS AND STRUCTURES

Institute of Materials and Structures
Rīga, Ķīpsalas iela 6A, LV-1048
Tel. +371 67089124
Web. http://www.ims.rtu.lv

The indenter displacement δ and contact zone size ρ at a given applied force are obtained as the values minimizing the total potential energy, Eq. (3.13). This can be done by seeking the stationary point of $\Pi(\delta, \rho)$

$$\begin{cases} \dfrac{\partial \Pi(\delta, \rho)}{\partial \delta} = 0 \\ \dfrac{\partial \Pi(\delta, \rho)}{\partial \rho} = 0 \end{cases} \qquad (3.14)$$

Although the first of the relations in Eq. (3.14) leads to an explicit expression for indentation force P in terms of indenter displacement δ and contact zone size ρ, the second relation still needs to be solved numerically. Alternatively, appropriate direct numerical minimization procedures can be applied to Eq. (3.13). Upon evaluation of δ and ρ, indentation radius a is obtained from Eq. (3.12).

3.2 Residual indentation

Consider a quasi-static unloading of the indented panel. During it, the indented face sheet partially rebounds. We make a simplifying assumption that the extent of BVID zone, characterized by its radius a, and overall shape Eq. (3.1) do not change during unloading as shown schematically in Figure 3.2, and the geometrical constraint Eq. (3.2) also holds.
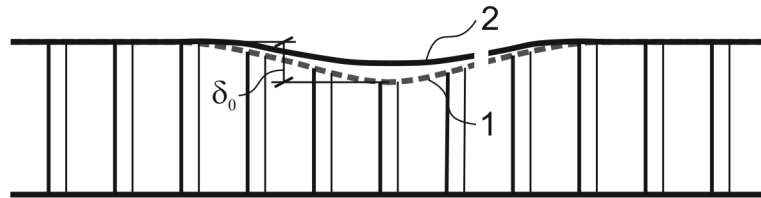
Figure 3.2. Schematic of indentation profiles at the end of active loading (1) and upon unloading (2).

The elastic energy of the face sheet at the end of active loading, U_0, is partially dissipated as the work of plastic deformation, D, of the core during unloading and partially retained as residual deformation energy of the face sheet U_r:

$$U_0 = U_r + D. \qquad (3.15)$$

Assuming that the tensile yield stress of the core is equal to the crush stress q and denoting the indentation profile at the end of active loading by w_0 and the residual indentation profile by w_r, the dissipated energy is expressed as

RIGA TECHNICAL UNIVERSITY
IMS
INSTITUTE OF MATERIALS AND STRUCTURES

Institute of Materials and Structures
Rīga, Ķīpsalas iela 6A, LV-1048
Tel. +371 67089124
Web. http://www.ims.rtu.lv

$$D = q \int\limits_{0}^{a} \int\limits_{0}^{2\pi} (w_0 - w_r) r \, d\varphi dr .$$ (3.16)

Both indentation profiles in Eq. (3.16) comply with Eq. (3.1), but for w_0 indentation depth δ_0 and contact zone radius ρ_0 reached at the end of active loading have to be used in Eq. (3.1), while for w_r - the residual values δ_r, ρ_r of the respective dent characteristics. Upon integration and substitution of indenter displacement by an expression following from Eq. (3.2)

$$\delta = \frac{2R\sqrt{R^2 - \rho^2} - 2R^2 + aR + a^2}{2\sqrt{R^2 - \rho^2}} ,$$ (3.17)

we finally obtain

$$D = \frac{1}{12}\pi q \frac{-8R^4 + 4R^2\rho_0^2 + 8R^3\sqrt{R^2 - \rho_0^2} + \rho_0(a + \rho_0)(a^2 + \rho_0^2)}{\sqrt{R^2 - \rho_0^2}} - \frac{1}{12}\pi q \frac{-8R^4 + 4R^2\rho_r^2 + 8R^3\sqrt{R^2 - \rho_r^2} + \rho_r(a + \rho_r)(a^2 + \rho_r^2)}{\sqrt{R^2 - \rho_r^2}}$$ (3.18)

Similarly, the expressions of strain energy are obtained from Eqs. (3.7), (3.8) upon substitution of Eq. (3.17) and of the respective contact zone radius value, leading to

$$U_0 = \frac{1}{64}\pi L \left(\frac{R^2\rho_0^2}{R^2 - \rho_0^2} + \rho_0^2 + 2R^2 \log\left(1 - \frac{\rho_0^2}{R^2} \right) \right) + \frac{1}{960}\pi L \frac{\rho_0^4(a - \rho_0)(a + 5\rho_0)}{(R^2 - \rho_0^2)^2}$$ (3.19)

and

$$U_r = \frac{1}{64}\pi L \left(\frac{R^2\rho_r^2}{R^2 - \rho_r^2} + \rho_r^2 + 2R^2 \log\left(1 - \frac{\rho_r^2}{R^2} \right) \right) + \frac{1}{960}\pi L \frac{\rho_r^4(a - \rho_r)(a + 5\rho_r)}{(R^2 - \rho_r^2)^2} .$$ (3.20)

Inserting the expressions Eqs. (3.18)-(3.20) into Eq. (3.15), an equation for ρ_r is obtained. Upon solving it numerically, depth of the residual dent can be evaluated from Eq. (3.17) as

RIGA TECHNICAL UNIVERSITY
IMS
INSTITUTE OF MATERIALS AND STRUCTURES

Institute of Materials and Structures
Rīga, Ķīpsalas iela 6A, LV-1048
Tel. +371 67089124
Web. http://www.ims.rtu.lv

$$\delta_r = \frac{2R\sqrt{R^2 - \rho_r^2} - 2R^2 + aR + a^2}{2\sqrt{R^2 - \rho_r^2}}. \tag{3.21}$$

3.3 Validation of analytical approach

The analytical model described above was validated against test results of aluminium honeycomb core/CFRP face sheet sandwich specimens subjected to quasi-static indentation to $P = 500$ N load by an indenter with a hemispherical tip of radius $R = 10$ mm. Two different face sheet lay-ups, [60/0/-60] and [0/60/-60/0], and sandwich support conditions, plate and frame, were considered as indicated in Table 3.1.

The designation "plate" in Table 3.1 denotes rigidly supported sandwich specimen during indentation, which was achieved by placing the specimen on a steel plate. Designation "frame" implies that the sandwich was supported only along its perimeter during indentation test by placing it on a steel frame. In the latter case, apart from the local deformation at the indenter, the sandwich also underwent global deformation by bending and shear. It has been demonstrated in, e.g., [10, 11, 12, 166], that the indenter tip displacement (equal to the top face sheet displacement under indenter) δ_A, in such a case can be represented as a sum of indentation depth and the global deflection of the sandwich (equal to the bottom face sheet displacement under indenter) δ_B. Since both top and bottom face sheet displacements along the line of indentation were recording during the tests with frame support of sandwich specimens, indentation depth at the maximum load was evaluated as

$$\Delta\delta = \delta_A - \delta_B$$

and the respective values reported in Table 3.1. The experimentally determined residual indentation depth and diameter are also reported in the table.

Table 3.1. Experimentally determined and predicted maximum indentation depth, residual depth, and diameter of indentation for sandwich panels subjected to 500 N load.

Designation	Facesheet lay-up	Maximum indentation depth		Residual indentation depth		Diameter 2a of indentation	
		$\Delta\delta$ exp., mm	δ_a, mm	δ_r exp., mm	δ_r theor. mm	Exp., mm	Theor. mm
ESA_003, frame	[60/0/-60]	1.02 (0.04)	1.04	0.44 (0.03)	0.48	17.5 (1.4)	23.1
ESA_003, plate		1.13 (0.10)		0.44 (0.04)		16.3 (1.7)	
ESA_016, plate	[0/60/-60/0]	0.93 (0.05)	0.95	0.40 (0.3)	0.41	16.8 (1.1)	23.1

Using the previously determined UD composite properties and the measured face sheet thickness, components of the in-plane stiffness matrix of the face sheets were evaluated by an elementary theory of laminates according to their lay-up and the parameter $L = 3A_{11} + 2A_{12} + 3A_{22} + 4A_{66}$ was estimated. *L* amounted to 108.7 MPa·m for face sheets of [60/0/-60] lay-up and 151.0 MPa·m for [0/60/-60/0] lay-up. The crushing stress of Al honeycombs was determined by flatwise compression tests at *q* = 1.6 MPa. The theoretical maximum indentation depth at the end of active loading, residual indentation depth and diameter were evaluated by the model described above and the values obtained presented in Table 3.1. The agreement of predicted and measured maximum indentation depth is reasonable, while the average residual indentation depth is slightly overestimated.
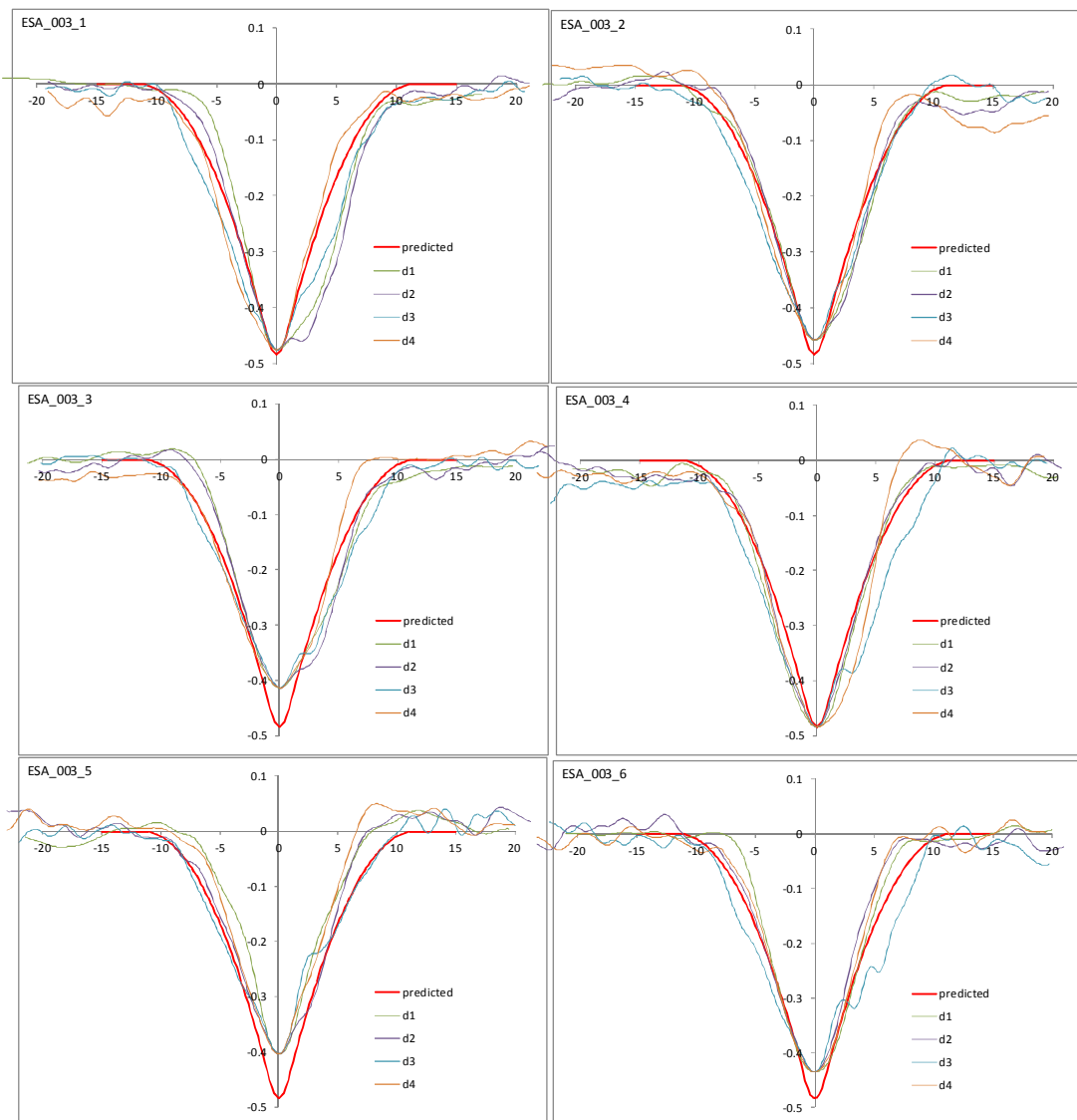

Figure 3.3. Comparison of experimentally determined and predicted residual indentation profiles for ESA_003 series sandwiches.

RIGA TECHNICAL UNIVERSITY

IMS

INSTITUTE OF MATERIALS AND STRUCTURES

Institute of Materials and Structures
Rīga, Ķīpsalas iela 6A, LV-1048
Tel. +371 67089124
Web. http://www.ims.rtu.lv

Although the predicted diameter of the dent appears to overestimate considerably the actual damage zone size as seen in Table 3.1, direct comparison of dent profiles in Figure 3.3. and Figure 3.4. demonstrates a rather good agreement. This suggests that the disagreement in the predicted and measured diameters is likely to be an artifact stemming from the measurement technique used in experimental determination of diameters.
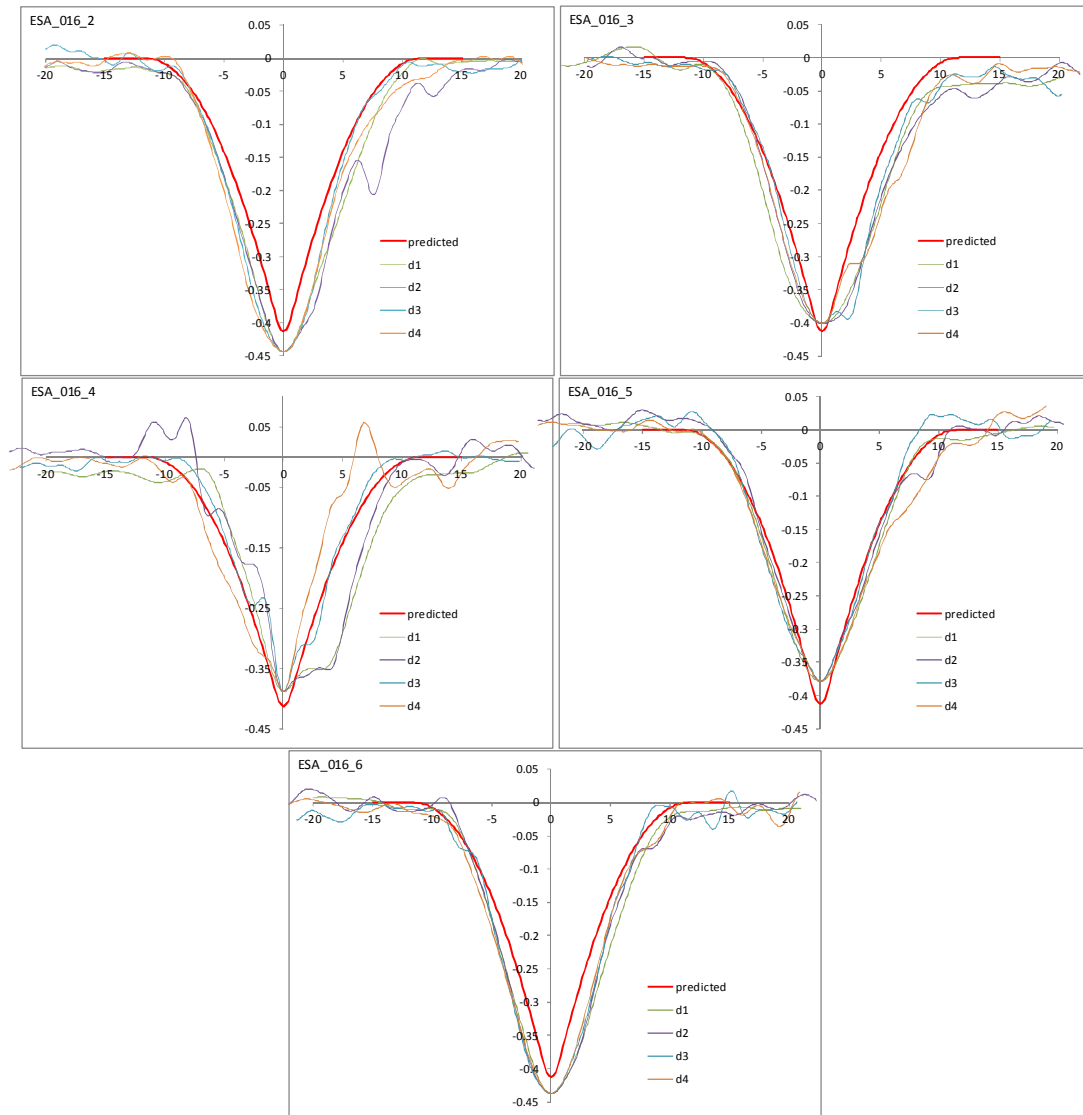

Figure 3.4. Comparison of experimentally determined and predicted residual indentation profiles for ESA_016 series sandwiches.

Figure 3.3. and Figure 3.4. present a more detailed view of the scatter in size and shape of residual indentation profiles along four planes intersecting at the lowest point of the residual dent of the same specimen, as well as scatter between specimens. The predicted indentation profiles appear to capture the overall shape of the dent reasonably well. For ESA 003 series ([60/0/-60] face sheet lay-up), the predicted dent is somewhat deeper than that observed for most of the specimens,

RIGA TECHNICAL UNIVERSITY
IMS■
INSTITUTE OF MATERIALS AND STRUCTURES

Institute of Materials and Structures
Rīga, Ķīpsalas iela 6A, LV-1048
Tel. +371 67089124
Web. http://www.ims.rtu.lv

see Figure 3.3. suggesting that the damage is overestimated, which would be likely to lead to a conservative CAI strength estimate based on the theoretical dent profile. However, for ESA 016 series ([0/60/-60/0] face sheet), predicted δ_r agrees within scatter with the average experimental dent depth, seeTable 3.1. hence overestimates the dent depth for some of the specimens and underestimates for the rest, as seen in Figure 3.4. The apparent overall agreement of the predicted residual dent profile with experimental data from two series of sandwiches, differing in face sheet lay-up, leads credence to the analytical modelling approach pursued.

RIGA TECHNICAL UNIVERSITY

IMS■

INSTITUTE OF MATERIALS AND STRUCTURES

Institute of Materials and Structures
Rīga, Ķīpsalas iela 6A, LV-1048
Tel. +371 67089124
Web. http://www.ims.rtu.lv

4   Conclusions

Current report outline a broad variety of numerical approaches which could be employed for numerical modelling of damaged sandwich panel uder compression force. A correlation of element mesh size as well as sensitivity analysis of assumed properties have been outlined. A dozen of validation cases have been drawn and alrady available on project web page under tool section: http://bnm4eks.rtu.lv/tools_en.html

5   Further work

Although BVID by definition does not imply massive damage to the sandwich structure, localized fracture of the face sheet plies and/or their delamination cannot be excluded even for BVID. Therefore, it is envisaged that strength of materials and/or fracture mechanics criteria for cracking onset and growth will be considered in the context of quasi-static and low-velocity impact loading of the composite face sheet of a sandwich. Appropriate means will be sought to allow for face sheet fracture in the analytical model of indentation so that the model does not become overcomplicated simultaneously providing reasonable accuracy of prediction. Also, the predictive capacity of the model in the case of low-velocity impact needs to be ascertained.

The next step in the analytical modelling will be estimation of CAI strength of impacted and indented sandwich panels with BVID. Developing models allowing for both, face sheet fracture and dent propagation modes will be aimed at.

Concerning progressive inwards buckling of the face sheet within and around the BVID region, the current modelling approach, although called analytical, relies heavily on numerical analysis methods including discretisation of the region to be modelled [18, 199] which renders their advantages over standard non-linear FEM modelling dubious. Therefore simpler analytical approaches will be sought and their accuracy evaluated against FEM results. Applicability of the localized wrinkling model [20] to sandwich panels with characteristics typical in ESA applications will also be considered.

Concerning evaluation of face sheet fracture loads in CAI as affected by BVID, analytical methods of estimation of stress concentration in the face sheet at the damage site based on the different assumptions and respective fracture criteria [21-24] will be analysed for their suitability with regard to specific Al honeycomb/CFRP sandwiches considered, with the aim of selecting the most appropriate analytical model for CAI strength.

RIGA TECHNICAL UNIVERSITY
IMS
INSTITUTE OF MATERIALS AND STRUCTURES

Institute of Materials and Structures
Rīga, Ķīpsalas iela 6A, LV-1048
Tel. +371 67089124
Web. http://www.ims.rtu.lv

References

1. *ANSYS® Academic Research, Release 16.2, Help System, Coupled Field Analysis Guide, ANSYS, Inc.*

2. Comparative evaluation of failure analysis methods for composite laminates, Final report of DOT/FAA/AR-95/109, Washington DC. 1996.

3. Brenda L. Buitrago, Carlos Santiuste, Sonia Sánchez-Sáez, Enrique Barbero, Carlos Navarro, Modelling of composite sandwich structures with honeycomb core subjected to high-velocity impact, Composite Structures, 92 (9) 2010: 2090-2096. http://dx.doi.org/10.1016/j.compstruct.2009.10.013.

4. ASTM D7766 - Standard Practice for Damage Resistance Testing of Sandwich Constructions

5. ASTM D7136 - Standard Test Method for Measuring the Damage Resistance of a Fiber-Reinforced Polymer Matrix Composite to a Drop-Weight Impact Event

6. ASTM E1876 - Standard Test Method for Dynamic Young's Modulus, Shear Modulus, and Poisson's Ratio by Impulse Excitation of Vibration

7. Cvitkovich MK, Jackson WC. Compressive Failure Mechanisms in Composite Sandwich Structures. *Journal of the American Helicopter Society* 1999; 44(4):260–268.

8. Kalnins K, Graham AJ, Sinnema G. Verification of residual strength properties from compression after impact tests on thin CFRP skin, Al honeycomb composites (2012) European Space Agency, (Special Publication) ESA SP, 691 SP, 7 p.

9. Czabaj MW, Zehnder AT, Davidson BD, Singh AK. Compressive strength of honeycomb stiffened graphite/epoxy sandwich panels with barely-visible indentation damage. *Journal of Composite Materials* 2014; 48(20):2455–2471.

10. Türk MH, Hoo Fatt MS. Localized damage response of composite sandwich plates. *Composites: Part B* 1999; 30:157–165.

11. Hoo Fatt MS, Park KS. Dynamic models for low-velocity impact damage of composite sandwich panels – Part A: Deformation. *Composite Structures* 2001; 52: 335–351.

12. Lin C, Hoo Fatt MS. Perforation of Sandwich Panels with Honeycomb Cores by Hemispherical-nose Projectiles. *Journal of Sandwich Structures and Materials* 2005; 7(2):133–172.

13. Lin C, Hoo Fatt MS. Perforation of Composite Plates and Sandwich Panels under Quasi-static and Projectile Loading. *Journal of Composite Materials* 2006; 40:1801-1840.

14. Chai GB, Zhu S. A review of low-velocity impact on sandwich structures. *Proceedings of the Institution of Mechanical Engineers, Part L: Journal of Materials Design and Applications* 2011; 225:207-230.

15. Khalili SMR, Hosseini M, Fard KM, Forooghy SH. Static indentation response of an in-plane prestressed composite sandwich plate subjected to a rigid blunted indenter. *European Journal of Mechanics A/Solids* 2013; 38:59-69.

16. Fard KM, Khalili SMR, Forooghy SH, Hosseini M. Low velocity transverse impact response of a composite sandwich plate subjected to a rigid blunted cylindrical impactor. *Composites: Part B* 2014; 63:111–122.

17. Feli S, Khodadadian S, Safari M. A modified new analytical model for low-velocity impact response of circular composite sandwich panels. *Journal of Sandwich Structures and Materials* 2016; 18(5):552–578.

18. Minguet PJ. A Model for Predicting the Behavior of Impact-Damaged Minimum Gage Sandwich Panels Under Compression. 32nd AIAA/ASME/ASCE/AHS/ASC Structures, Structural Dynamics and MaterialsConference, 1991, 1112-1122.

19. Xie Z, Vizzini AJ. Damage Propagation in a Composite Sandwich Panel Subjected to Increasing Uniaxial Compression after Low-velocity Impact. Journal of Sandwich Structures & Materials 2005;7: 269-288.

20. Staal RA, Mallinson GD, Jayaraman K, Horrigan DPW. Predicting Failure Loads of Impact Damaged Honeycomb Sandwich Panels. Journal of Sandwich Structures and Materials 2009 11: 213-244.

21. Kassapoglou C. Compression strength of composite sandwich structures after barely visible impact damage. *Journal of Composites Technology and Research* 1996; 18(4):274-284.

22. Ratcliffe J, Jackson W, Schaff J. Compression strength prediction of impact-damaged composite sandwich panels. Annual Forum Proceedings - American Helicopter Society, 2004, Vol. 1, 656-672.

23. Ransom JB, Glaessgen EH, Ratcliffe JG. An Overview of Durability and Damage Tolerance Methodology at NASA Langley Research Center. In: Advances in Interdisciplinary Mathematical Research, Springer Proceedings in Mathematics & Statistics, 2013, Volume 37, pp.1-34.

24. Kassapoglou C. Impact. In: Modeling the Effect of Damage in Composite Structures: Simplified Approaches, 2015, 105-169.